Coordination Chemistry Reviews 480 (2023) 215025

Contents lists available at ScienceDirect

Coordination Chemistry Reviews

journal homepage: www.elsevier.com/locate/ccr

Review

Hybrid nanostructures based on gold nanoparticles and functional coordination polymers: Chemistry, physics and applications in biomedicine, catalysis and magnetism

Roger Sanchis-Gual [a], Marc Coronado-Puchau [a,b], Talal Mallah [c], Eugenio Coronado [a,*]

[a] Instituto de Ciencia Molecular, Universitat de València, Catedrático José Beltrán 2, 46980 Paterna, Spain
[b] Departamento de Medicina. Universitat de València, Av. Blásco Ibáñez, 15 46010 Valencia, Spain
[c] Institut de Chimie Moléculaire et des Matériaux d'Orsay, Université Paris-Saclay, CNRS, 91405 Orsay Cedex, France

ARTICLE INFO

Article history:
Received 20 July 2022
Accepted 8 January 2023

Keywords:
Gold nanoparticles
Colloidal chemistry
Coordination chemistry
Prussian Blue
Spin crossover
Metal–organic framework

ABSTRACT

During the last decade, the scientific community has become interested in hybrid nanomaterials, especially the ones that combine gold nanoparticles with a second functional component. In this context, coordination polymers are materials that possess potential advantages over conventional inorganic nanomaterials and organic compounds such as chemical versatility, easy processability, high specific area, low toxicity, biodegradability and electronic and magnetic functionalities to name a few. In this manner, the wise integration of Au nanoparticles with coordination polymers in different types of nanostructures has allowed extending the scope of properties and applications of these systems, allowing also overcoming some of the limitations of Au nanoparticles for certain applications. Therefore, in this review, we discuss the different reported hybrid nanostructures based on the integration of colloidal Au nanoparticles with coordination polymers exhibiting either physical properties of interest (*e.g.* ferromagnetism, photomagnetism, spin switching, etc.) or chemical properties (*e.g.* electrocatalysis). We have paid particular attention to the enhanced properties and the synergistic effects that can emerge from this association. Along this front, thanks to their improved and/or novel properties, these hybrid materials have become promising nanostructures for several applications, especially in biomedicine, catalysis, magnetism and sensing.

Contents

* Corresponding author.
E-mail address: eugenio.coronado@uv.es (E. Coronado).

https://doi.org/10.1016/j.ccr.2023.215025
0010-8545/

1. Introduction

An appealing possibility in materials chemistry is to design nanoparticles (NPs) of hybrid nature by combining a metallic NP, in particular gold ones, with other types that bring an additional physical or chemical function. The mutual interaction (electronic, structural, etc) between the two components of the nanostructure may lead to the emergence of novel functions stemming from synergetic effects beyond the mere combination of the physicochemical properties of the two components.

In this context, colloidal chemistry is a powerful approach that offers advantages over other methods for the development of hybrid nanostructures such as high particle stability, a large exposed surface area and a precise chemical control of the particle size, shape, composition, structure, and crystallinity [1,2]. The combination of colloidal NPs with other functional nanomaterials into advanced materials with targeted physical and/or chemical properties may create novel functions at the nanoscale and can extend the scope of the utilization of these hybrid nanomaterials [3]. In this sense, most of the research effort has been focused on the combination of Au NPs with metal oxides or with organic compounds [4–7]. Yet, the utilization of coordination polymers (CPs) as a functional material for these hybrid nanostructures is a burgeoning research field in inorganic chemistry and materials science [8–11].

The current interest of the scientific community in hybrid NPs is reflected in the number of publications per year, which has increased up to 5000 in 2021 (Fig. 1). A significant part (*ca.* 15 % of the total number of publications in the last 5 years) involves hybrid materials containing Au NPs, from which 30 % contain CPs as a functional molecular component. Hence, the design of multifunctional hybrid NPs formed by combining Au with CPs represents the most active focus of interest in this area.

Therefore, this review aims to cover the new advances performed on Au NPs-CPs hybrid nanostructures exhibiting either physical properties of interest (ferromagnetism, photomagnetism, spin switching, etc.) or chemical properties (electrocatalysis). Particular attention will be paid to the synergistic effects that can appear due to this association. The choice of CPs in these hybrid nanostructures is based on their structural and chemical versatility, easy processability, high specific area, good solubility, low toxicity and biodegradability [12]. Here we will focus on three types of coordination polymers, namely Prussian Blue Analogues (PBAs), Spin Crossover materials (SCOs) and Metal-Organic Frameworks (MOFs). The former two provide examples of magnetic and electroactive materials of major interest in magnetism and electrocatalysis, while the last one provides the opportunity to add porosity to the hybrid nanostructure.

2. Gold nanoparticles

In 1857, Michael Faraday investigated a "beautiful ruby fluid" obtained from the formation of a deep red-colored colloidal Au by the reduction of an aqueous solution of gold chloride ($AuCl_4^-$) [13]. Faraday realized that the color was necessarily caused by the small size of the Au particles. He correctly supposed that the metallic particles in the colloids should be very small because they could not be observed with the best available microscopes. He also noted that their colors ranged from ruby, green, violet and blue depending on the composition of the metallic particle. Approximately a century later, the shorter wavelengths generated in electron microscopes evidenced that Faraday's Au colloids had diameters from 3 to 30 nm [14]. Then, Gustav Mie, using Maxwell's electromagnetic theory, provided at the beginning of the twentieth century a general theory for scattering and absorption of light by spherical metallic particles [15]. In 1912, Richard Gans generalized Mie's result to ellipsoidal particles of any aspect ratio in the small particle approximation [16]. Furthermore, the advancement in transmission electron microscopy imaging led to a renaissance in the investigation of the structure and morphology of metal colloids allowing the investigation and exploitation of their properties.

The above observations emphasized how physical properties at the nanoscale are notably different from those observed in the bulk (macroscopic). In fact, the drastic changes observed in the optical behavior, by reducing the size of metallic particles —hardly

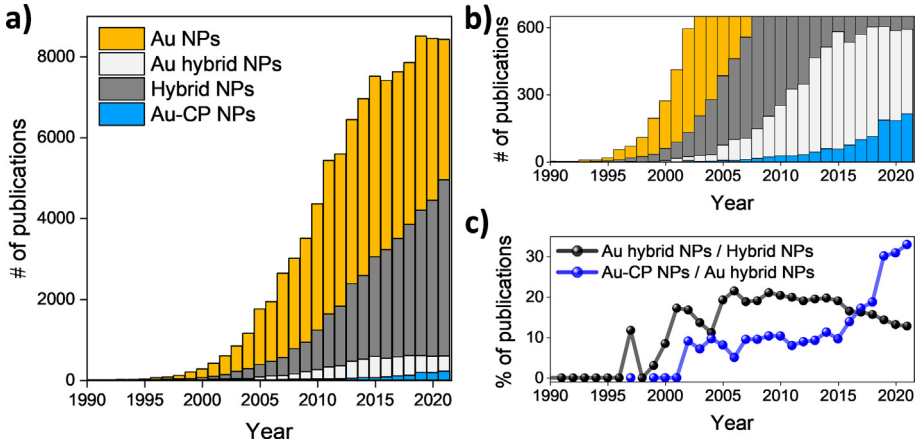

Fig. 1. a) Number of publications containing the terms "gold nanoparticles", "hybrid gold nanoparticles", "hybrid nanoparticles" and "gold coordination polymers nanoparticles" since 1990. b) Zoom of Fig. 1a. c) Percentage of publications of Au-hybrid NPs/Au NPs and Au-CP NPs/Au Hybrid NPs since 1990. Source: Scopus, as assessed in April 2022.

achievable in other optical materials— are due to the surface plasmon resonance. A plasmon is defined as a quantum oscillation of the free electron cloud with respect to the fixed positive ions in a metal and those that are confined on surfaces and strongly interacting with light are called surface plasmons. In this context, localized surface plasmon resonance (LSPR) is a phenomenon that takes place in Au NPs. In general, when the electromagnetic radiation interacts with a spherical metallic nanostructure much smaller than the wavelength of the light used to excite the plasmon, the electrons near a metal-dielectric interface are excited (Fig. 2). Then, these electrons undergo collective oscillations relative to the fixed positive nuclei, with the frequency of the incoming light. A local electric field is generated on the surface of the NP as a result of these oscillations. This effect can be extended into the dielectric over nanometer lengths and generates an enhancement of the incident field of several orders of magnitude. Note that the resonant frequency for these oscillations in spherical noble metallic NPs corresponds typically to UV–Vis light, and hence the LSPR produces absorption bands in this region of the spectrum. In this regard, the resonant frequency is influenced by various factors such as the metallic composition, the size, the shape and the surroundings of the NPs [17–20]. For example, the LSPR of 20 nm Au NPs can be experimentally observed in water at a wavelength of 520 nm and red shifts to 600 nm as the NP diameter increases to 100 nm [21]. On the other hand, anisotropic NPs can display different resonant frequency modes. In the case of nanorods (NRs), their spectra exhibit two plasmon bands associated with LSPRs along their length and across their diameter (longitudinal and transversal resonances, respectively). These frequency resonances related to anisotropic NPs (*e.g.* the longitudinal mode for the NRs) are much more sensitive than the LSPR from spherical NPs and have been extensively applied for sensing [22,23].

Among other applications, plasmons can be used to enhance the local electric field (for example, for Surface Enhancement Raman Spectroscopy (SERS) detection), to produce a local heat (photothermal effect), or even to detect color (plasmon sensibility). Considering the unique features of Au (such as the amenable surface functionalization, the low cytotoxicity, the high stability, and the electrical and thermal conductivity), Au NPs exhibit numerous exciting properties that have permitted the development of successful new applications in materials science, electrochemistry or biomedicine, to mention a few [6,14,25–28]. For example, Au NPs are widely used in catalysis, and Au catalysis represents a paradigmatic example of those properties exclusively observed in NPs because they can completely disappear when the particle size grows into the microscale [29,30]. Au NPs are commonly chosen because of their good biological compatibility, excellent conducting capability, and high reactivity due to the high surface-to-volume ratio. Applications of Au NPs in electrochemistry can be found including Au NPs-based sensors and their use as an enhancing platform for electrocatalysis [31]. Concerning their usage in biomedicine, small NPs are highly desirable because they can be depurated much more easily. However, for photo-therapy, Au nanospheres have poor near-infrared (NIR) absorption, which is necessary to avoid damaging cell tissues. Hence, the development of anisotropic Au NPs with suitable optical properties and shapes is crucial [32,33].

The exploitation of the unique properties of Au NPs relies on the development of chemical methods permitting a control over the size, shape and morphology of the nanostructures. In general terms, this involves the use of colloidal methods in which the Au NPs are made by assembling Au atoms generated from ions in solution. Typically, Au NP obtained by using this approach comprises three parts, namely inner Au atoms (central atoms), atoms exposed to the surface (surface atoms) and surface-protecting organic ligands or surfactants. The central Au atoms determine the crystallinity of the nanostructure, whereas the structure of the surface atoms form surface facets and edges that will dictate their reactivity, including the catalytic activity. The surfactant is anchored on the surface atoms, stabilizing them and providing surface functionality [25].

The first achievement in this context was the preparation of spherical Au NPs and later on, of NPs of various anisotropic shapes including nanorods, nanoshells, and nanocages [26,34–38]. Thus, in 1951 Turkevich and coworkers established a synthetic method for creating spherical Au NPs by treating hydrogen tetrachloroaurate ($HAuCl_4$) with citric acid in boiling water (Fig. 3a); here the citrate act as both reducing and stabilizing agent [39]. In a further step, Frens in 1973 extended this protocol by changing the Au:citrate ratio to control the NP size from 10 to 20 nm [40], and then up to 100 nm [6]. Interest in the shape-controlled synthesis of Au nanostructures started in the early 1990s when Masuda et al. and Martin prepared AuNRs by electrochemical reduction. These methods produced relatively monodisperse nanostructures, but due to the low yield and large diameter (in the 100 nm range), the optical response was difficult to discern [25,41,42]. A decade after, a colloidal growth route based on a seeded growth method led to high yield monodisperse AuNRs (Fig. 3b). This seed-mediated growth involved two consecutive steps: i) the production of single-crystal spherical seed particles and ii) the controlled and guided growth of these seeds into anisotropic particles. By controlling these growth conditions in aqueous surfactant media, it was possible to synthesize AuNRs with a tunable aspect ratio (length/width). Thus, by modifying the NR length, the longitudinal

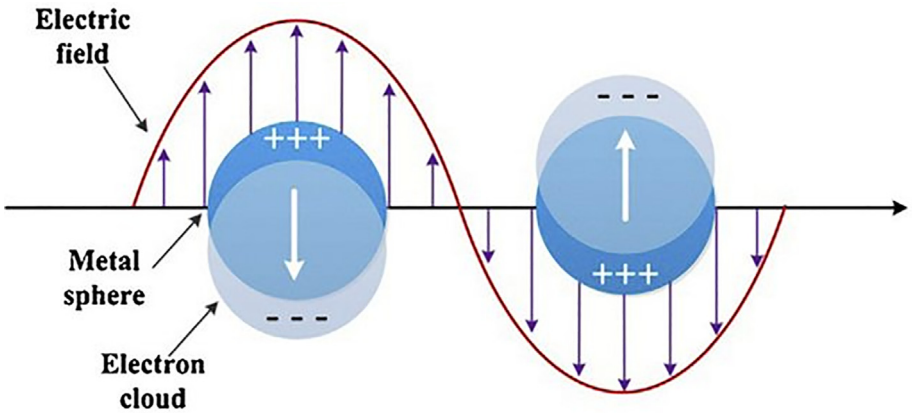

Fig. 2. Schematic illustration of a plasmon oscillation in a metallic sphere, showing the oscillations of the conduction electron cloud relative to the positive nuclei. Adapted from [24].

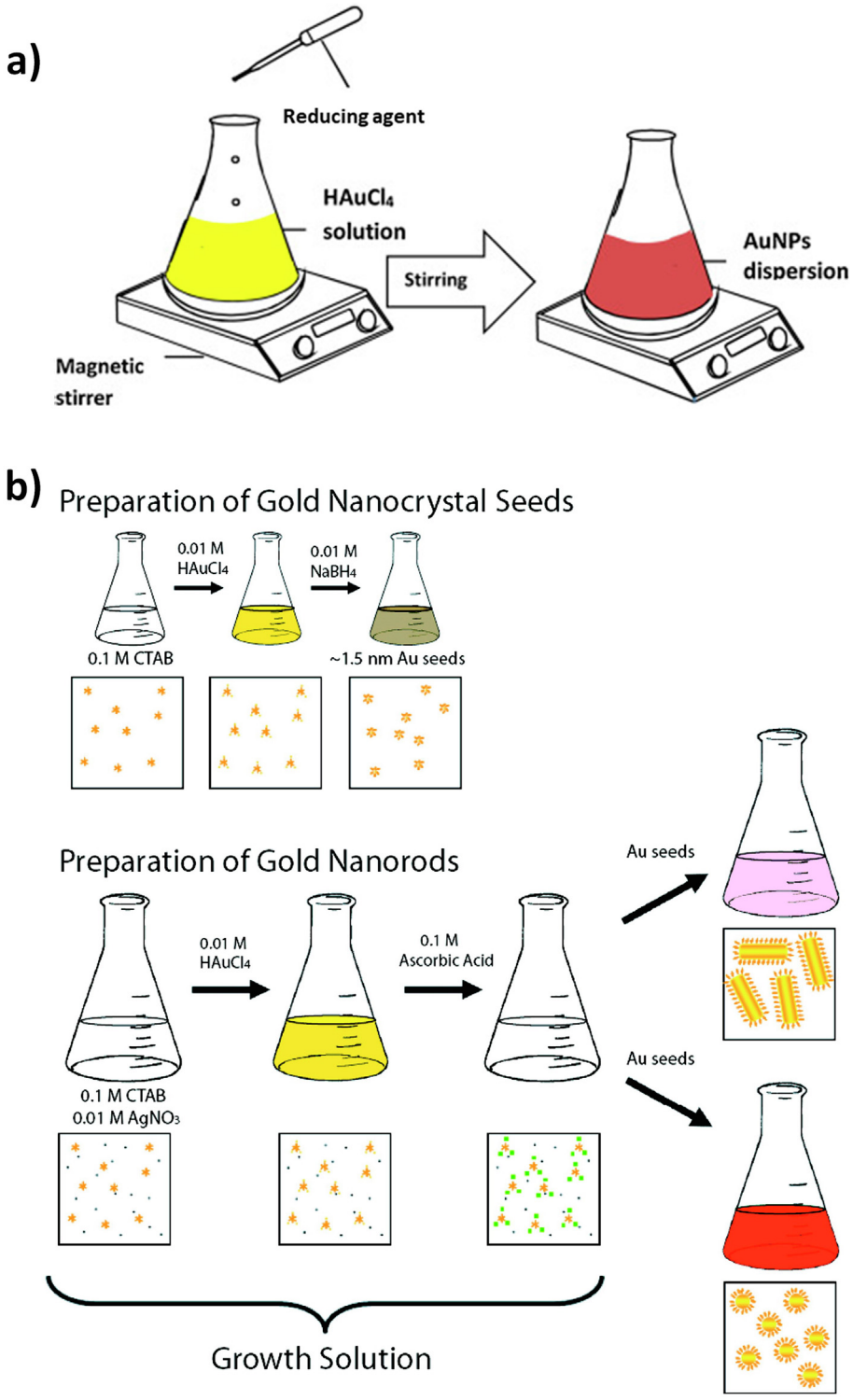

Fig. 3. a) Schematic illustration of Au NP preparation using a reducing agent. Adapted from [47]. b) Seed-mediated, surfactant-assisted AuNR synthesis. NR aspect ratio can be modified by adjusting the Ag concentration. Adapted from [48].

resonance can be modulated in part of the visible spectrum and in the NIR region, which is suitable for their usage in biomedicine [25,43,44].

Thanks to the high control over the particle synthesis, the seed-mediated growth has become the most widely used strategy in the preparation of anisotropic NPs of different shapes and sizes [45]. For instance, in 2008, Huang and coworkers used this method for the synthesis of gold nanostars (AuNSs) [46]. These nanostructures have plasmon bands that are tunable into the NIR region, with the NP containing multiple sharp branches that act as "hot spots" and greatly enhance the local electromagnetic field [35,46].

3. Functional coordination polymers

Even if the term "coordination polymer" started to appear at the end of the 20th century, the current extensive interest in CPs was triggered after the reports of Robson, Hoskins and coworkers in the

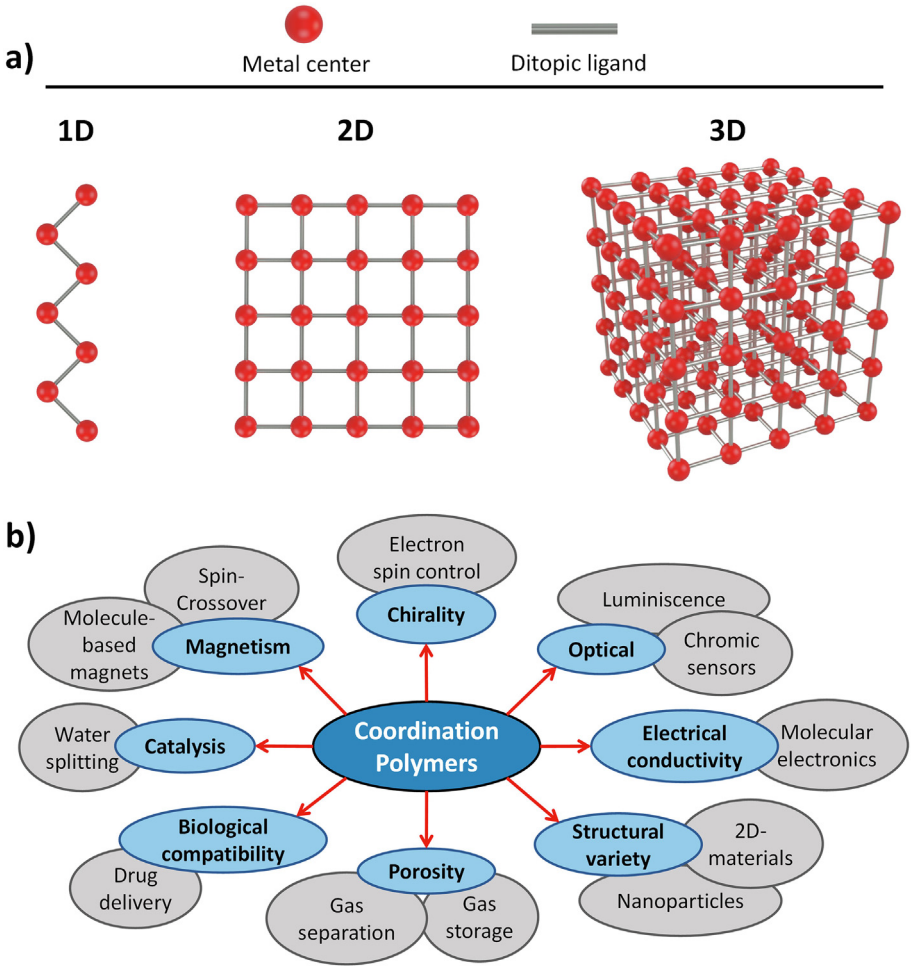

Fig. 4. a) Classification of coordination polymers depending on the dimensionality. b) Scheme showing the most relevant properties and applications of coordination polymers.

early 1990s [49,50]. A CP is a material that has a polymeric structure built from the association of metal ions and bridging organic linkers (ligands) forming coordination bonds that extend in one, two or three directions of space leading to networks with different dimensionalities. The wide variety of metal cations and ligands affords a vast number of possible combinations and, therefore, structures and topologies (Fig. 4a). The judicious choice of metals and ligands is crucial for obtaining a targeted structure [51–53].

The metal ions are usually d-transition metals and/or lanthanides. Generally, d-transition metals have been more popular due in part to the relatively predictable nature of their coordination geometries. For d-transition metals, the field is dominated by the first-row elements (plus Zn, Cd, Hg, Ag and, to a less extent, Au, Pd, Pt). Their low cost, earth abundance, kinetic lability and stability explain why the research on these d-transition metal-containing CPs is predominant compared to the rest [53]. When transition metal ions of the first row are used, magnetic and optical, in addition to catalytic properties, can be present, leading to a wide range of applications (Fig. 4b). Finally, nanostructures of these CPs can be prepared by using several synthetic protocols, including colloidal chemistry [52].

3.1. Prussian Blue analogues

Prussian Blue (PB) is an early example of functional CP. Its structure has a face-centered cubic (fcc) unit cell with alternating octahedral Fe^{III} and Fe^{II} bridged by the cyanide ligands and with the formula $Fe^{III}[Fe^{II}(CN)_6]\cdot nH_2O$. Its intense blue color is due to an intervalence charge transfer band associated with the Fe^{II}-CN-Fe^{III} mixed-valence unit [53–55]. Replacing Fe^{III} or Fe^{II} with other transition metal ions gives rise to Prussian Blue Analogues (PBAs) of general formula $A_aB_x[D(CN)_6]_y\cdot nH_2O$ (A = alkali cation, B and D = transition metal ions), which possess the same cubic structure (Fig. 5a). These networks are usually prepared by mixing a hexacyanometalate ($[D(CN)_6]^{n-}$) that plays the role of the ligand with $[B(H_2O)_6]^{m+}$ affording bimetallic networks whose magnetic and optical behavior can be tuned by the nature of the metal ions. The tetrahedral sites of the fcc structure may be filled by alkali ions (such as Cs, Rb) that compensate for the negative charge of the network. The absence of such alkali ions leads to vacancies in hexacyanometalate species and therefore to remaining water molecules in the coordination sphere of the B metal ions. Vacancies lead to the presence of channels within the 3D network that are usually filled with a network of H-bonded water molecules [53,56,57]. The concentration of vacancies and alkali ions highly impacts the magnetic and the optical properties of PBA analogues and can be used to finely tune them [58–61]. Indeed, most PBAs behave as molecular magnets thanks to their bimetallic nature that promotes tunable magnetic exchange coupling between the different spin carriers mediated by the cyanide bridge [62,63]. These features have allowed to push up the magnetic ordering temperatures from 5 K in PB to room temperature in a VCr containing PBA [55]. Photomagnetic properties were also discovered in the CoFe containing PBA where a conversion from a diamagnetic to a magnetic

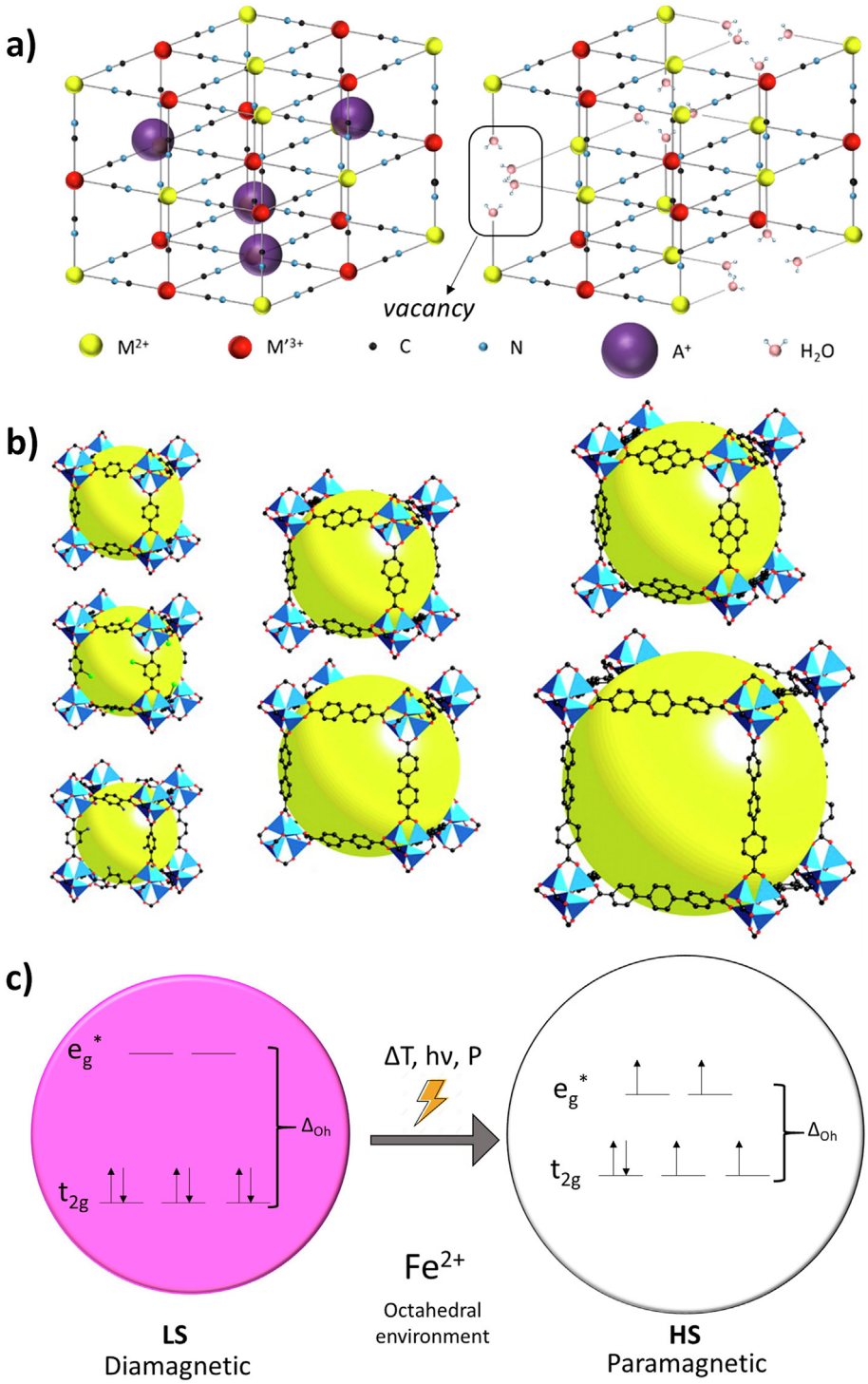

Fig. 5. Details of the three reviewed CPs. a) Illustrations of the cubic structure of the PBA (left) and the PBA with random site defects (right). The appearance of defects leads to a lower amount of alkali metals due to charge balance. The PB structure is identical but Fe^{II} centers are connected to C atoms while Fe^{III} centers are connected to N atoms. b) Pore sizes of a MOF depending on the ligand used. The large yellow spheres represent the largest van der Waals spheres that would fit in the cavities without touching the frameworks. c) Example of the SCO phenomenon for a Fe^{II} compound in an octahedral environment. The spin transition involves switching from a diamagnetic (LS) state to a paramagnetic (HS) state. Fig. 5b was adapted from [121]. (For interpretation of the references to color in this figure legend, the reader is referred to the web version of this article.)

state could be triggered by light excitation [57]. Thanks to the open framework structure induced by the hexacyanometalate vacancies, the large specific surface area, the adjustable metal active sites, the uniform catalytic centers and the high chemical and electrochemically stability, these compounds are also very promising materials for different catalytic reactions [64,65].

All these physical and chemical properties can be exploited at the nanoscale thanks to the preparation of nanoparticles of PB and its PBA. These objects can be prepared as colloids that are stable in water for several years, and, depending on the synthetic conditions, their size can be tuned over a large range *i.e.* from 2 to 200 nm [54,66]. This versatility has allowed the production of

PBAs in various shapes and sizes, including individual NPs [54], hollow nanostructures [67], films [68], wires [69] and even core@-shell particles formed by combining two or three different PBAs [66], or a PBA with another different material [70]. It is important to remark that there is an increasing interest in combining PBAs with other inorganic materials in order to form multifunctional nanosystems exhibiting synergistic chemical and physical properties that lead to the emergence of new functions [71,72]. For example, PBAs have a strong charge-transfer absorption that can be used to undergo thermal relaxation and can be exploited to generate local hyperthermia by light irradiation. In addition, these CPs are colloidally stable, fully biocompatible (PB use has already been approved by the FDA), biodegradable and easy to be functionalized, making them ideal candidates for biomedical applications [73–75].

3.2. Metal–Organic Frameworks

Porous CPs, also known as Metal–Organic Frameworks (MOFs), are a promising class of coordination materials where the combination of the metal centers and the organic ligands gives rise to reticular networks with high crystallinity, ultrahigh pore volumes (up to 90 % free volume) and extremely large specific surface areas (extending beyond 6000 m^2/g) [76]. From a chemical point of view, it is important mentioning that many different possible synthetic routes, which include room temperature synthesis, conventional electric heating, microwave heating, electrochemistry, mechanochemistry and ultrasonic methods, have been established [77]. Thanks to the exceptional chemical control over the structure, the tunability of the properties is possible. Thus, MOFs have emerged as a significant class of nanoporous materials with potential applications in gas storage, separation, catalysis, and chemical sensing [78–81].

In the present context, nanoscale MOFs combine small dimensions with the possibility to design highly porous architectures with well-defined and uniform sizes and morphologies in order to, for example, disperse them in aqueous media or other solvents, and to efficiently coat them for improving their biocompatibility or recognition capabilities. Still, porosity is not the only property that can be exploited. The possibility of introducing functional properties in the MOF, such as electrical conductivity, optical properties (*e.g.* plasmonic properties) or magnetism, is also very promising to expand the range of applications of these materials [82]. In this line, a hybrid approach in which a functional nanostructure is mixed with the MOF can be a valuable way to improve the properties of the MOF. For example, the encapsulation of active guest compounds inside MOFs is very promising to reach properties beyond those of the bare MOFs and/or guest species [83]. With this aim, a wide range of functional inorganic materials, including metallic NPs [84], coordination complexes [85], quantum dots [86], polyoxometalates [87] and even other MOFs [88], have been combined with MOFs to enhance their properties.

3.3. Spin crossover compounds

The SCO compounds provide the most spectacular example of molecular bistability [89]. This arises from the ability of a metal ion with a d^4 to d^7 electronic configuration to be switched between two electronic states, the high spin (HS) and the low spin (LS), in a readily detectable and reversible way (Fig. 5c). The transition between these two states may be typically induced by means of a variation of temperature, pressure, or light irradiation. This phenomenon induces changes in metal-ligand bond distances due to the population or depopulation of the e_g^* orbitals that have a slight antibonding character [90–92]. Therefore, the spin transition involves a compression/expansion of the coordination site. Reversible changes in their optical, magnetic, mechanical, and electrical properties also occur, making these compounds promising as molecular switches [93], optoelectronic devices [94], actuators [95], and sensors [96]. The archetypical transition metal compounds that may present SCO are octahedrally coordinated Fe^{2+} complexes. Some of them are CPs comprising 1D chains [97], 2D [98] and 3D networks [99], which may exhibit abrupt and/or hysteretic thermal spin transitions [92]. A key example of SCO CP was provided by the triazole chain compounds $[Fe(Htrz)_2(trz)](BF_4)$ first reported by Haasnoot et al. [100] and then studied by Kahn et al. [90]. These systems exhibit large and abrupt thermal hysteresis near room temperature, while allowing to obtain very small NPs that maintain the cooperative behavior [101,102]. The works reported in 2008 [103–106] on the synthesis of small SCO NPs motivated intense research in this area giving rise to the development of diverse protocols for the production of this kind of nanomaterials and their integration in hybrid nanostructures [107], as well as for the measurement at the nanoscale of the properties. In Table 1 we summarize the different achievements reported for the SCO triazole chains: 1) Synthesis of SCO NPs with sizes in the range below 100 nm by using the inverse micelle technique; 2) Synthesis of *ca.* 90 and 140 nm NPs covered with a thin layer of silica which enables their further surface functionalization and their integration on electronic devices; 3) Electrical spin switching measured in a single SCO NP; 4) Electrical spin switching sensed in a layered array of NPs using gold or graphene electrodes; 5) Electrical spin switching sensed in a hybrid heterostructure formed by SCO NPs deposited on a graphene layer; 6) Sensing of the spin transition in $SCO@SiO_2$ NPs by means of micromechanical resonators; 7) Synthesis of Au@SCO core@shell NPs with enhanced electrical sensing of the spin switching; 8) Fabrication of SCO@polymers nanocomposites for mechanical actuators upon electrical stimulus; 9) Optical spin switching sensed in a hybrid heterostructure formed by SCO NPs anchored on MoS_2 layers.

At this point, it is worth noting that other CPs exhibiting network structures such as Fe(II) Hofmann clathrates are also of interest in this context since they display SCO along with the outstanding chemical robustness and, in some cases, selective

Table 1
Main achievements reported for the iron triazole based SCO NPs.

Compound	Achievement	Year	Reference
$[Fe(Htrz)_2(trz)](BF_4)$	Synthesis of SCO NPs	2008	[103,105]
$[Fe(Htrz)_2(trz)](BF_4)@SiO_2$	Synthesis of NPs covered with a thin SiO_2 layer	2011	[108]
$[Fe(Htrz)_2(trz)](BF_4)$	Electrical spin switching measured in a single NP	2011	[93]
$[Fe(Htrz)_2(trz)](BF_4)$	Electrical spin switching sensed in a layered array of NPs using gold or graphene electrodes	2015–2016	[109,110]
$[Fe(Htrz)_2(trz)](BF_4)$	Electrical spin switching recorded in SCO NPs deposited on a graphene layer	2017	[111]
$[Fe(Htrz)_2(trz)](BF_4)@SiO_2$	Sensing of the spin transition by means of micromechanical resonators	2019	[112]
$Au@[Fe(Htrz)_2(trz)](BF_4)$	Synthesis of Au@SCO core@shell NPs and electrical sensing of the spin switching	2019	[113]
$[Fe(Htrz)_{1.8}(trz)(NH_2trz)_{0.2}](BF_4)$@PVDF-TrFE	Integration of SCO NPs in polymers for mechanical actuators	2021	[114]
$[Fe(Htrz)_2(trz)](BF_4)@SiO_2/MoS_2$	Optical spin switching sensed in $SCO@SiO_2$ NPs anchored on MoS_2 layers.	2021	[115]

response to different molecules. The general formula of this family is $\{Fe(L)[M^{II}(CN)_4]\}\cdot G$ (L = bismonodentate pyridine-like ligand; M^{II} = Ni, Pd, Pt; G = guest) and $\{Fe(L)[M^{I}(CN)_2]_2\}\cdot G$ (M = Cu, Ag, Au). In both cases, the polycyanide linkers afford reticular 2D networks connected by a pillar ligand to give a 3D network. The square-planar $[M^{II}(CN)_4]^{2-}$ units generate 2D networks with small meshes preventing the interpenetration of the 3D networks and thus, favoring the formation of voids/pores between bridging pillar ligands, accessible for guest molecules. In this way, their SCO behavior is remarkably dependent on guest molecules, stabilizing in many cases the HS or the LS state depending on the absorbed molecules. Therefore, these materials have potential applications in molecular sensing [116,117]. Nanoscale architectures of these materials have been reported [118] and, taking advantage of their layered structure, they have been combined with other 2D materials, such as graphene and 2D semiconductors (WSe_2), to afford hybrid heterostructures exhibiting spin sensing [119]. However, very few combinations with plasmonic NPs have been reported so far [120].

4. Hybrid gold nanoparticles/coordination polymer nanostructures

4.1. Different structures

The design of hybrid nanostructures combining gold NPs with functional coordination polymers is a promising way toward multifunctional nanomaterials. Thus, as already mentioned, these nanostructures can feature a simple combination of physical or chemical properties, or display novel properties due to the mutual interactions between the two components. In addition to this, the functional components can lead to unique synergy-induced properties in the resulting hybrid material [122,123]. Several hybrid systems that combine inorganic materials with CPs have been investigated because of their enhanced catalytic activity [124], or because of the association of magnetic or optical properties coming from the inorganic NPs, with the porosity [23,125], electrical [115], electrochemical [65] or magnetic properties [126,127] coming from the CPs. Therefore, the controllable integration of metallic NPs and CPs into advanced hybrid materials with targeted functions can extend the scope of the utilization of these materials.

The combination of Au and other nanomaterials gives rise to different nanostructures (core@shell, Au-coated, yolk@shell, NP decoration, dumbbell/Janus, etc.) with some peculiarities. To have a better scope of the typical hybrid Au nanostructures, a classification of these nanoobjects is presented in Fig. 6. Depending on the targeted properties, a given hybrid nanostructure will be the most suitable. Besides, the corresponding synthetic strategy must focus on the development of these nanomaterials in a simple, efficient and sustainable way. Colloidal chemistry has advantages over other methods because it relies on the preparation and/or the use of isolated particles, which allows access to the whole particle. Furthermore, the particles are surrounded by a layer of organic ligand molecules and their hybrid nature greatly broadens the possibilities for tailoring their properties because both components can be manipulated independently [128]. In this way, colloidal chemistry has become a reliable approach for obtaining high quality hybrid NPs with precise control over their size, shape, composition and properties. The most common hybrid nanostructures formed by Au NPs and a functional material are displayed in Fig. 6:

(i) Core@shell nanostructures: These are highly functional nanomaterials whose properties, arising either from the core or from the shell, can be modified by modulating the core/shell size ratio. Thus, different synthetic approaches have been developed using a plethora of different procedures such as precipitation, grafted polymerization, microemulsion, reverse micelle, sol–gel condensation, layer-by-layer adsorption technique and so on. However, it is still difficult to control the thickness and homogeneity of the coating. The shell formation requires highly controlled and sensitive synthetic protocols to ensure complete coverage of the core. Thus, if this reaction is not properly controlled, it may lead to the aggregation of core particles, the formation of separate particles, or to an incomplete coverage [129]. Interestingly, some synthetic routes permit to achieve core@shell NPs using anisotropic Au NPs (rods, stars, cages, etc) [130,131] and multishell heterostructures [126,132] (*i.e.* core having several shells around them), thereby, allowing the chemists to modulate the LSPR of the system. Due to the close contact between these two nanosystems, the core@shell structure presents the largest interface area, thus facilitating the interaction between the two components. In

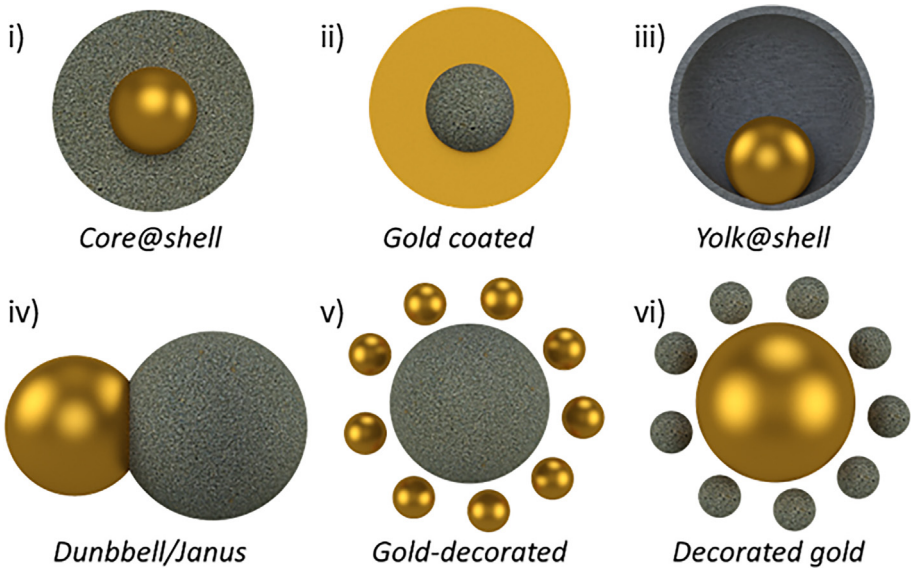

Fig. 6. The most common hybrid nanostructures formed by Au NPs and a functional material.

addition, it is important to point out that the Au core is entirely covered by the shell, thus protecting the Au core from the environment.

(ii) Gold-coated nanostructures: in contrast to the previous one, in this case, Au is used for covering NPs of different nature. Au confers plasmon properties, high chemical and colloidal stability and amenable surface functionalization that results in particular interest in biomedicine. Nevertheless, for such heterostructures, the core NP stands chemically inert and only the Au shell is able to interact with the environment. For this reason, these heterostructures are not appropriate when using CPs as the core NP, since they often require to interact with the environment. In fact, to the best of our knowledge, this type of heterostructure has not been obtained with CPs.

(iii) Yolk@shell NPs: These particles are a mixture of core@shell and hollow ones, where a core particle is encapsulated inside the hollow shell and may move freely inside the shell, generally represented as a core/void/shell. The yolk@shell nanostructures are also termed as movable core/shell or rattle-type nanostructures [133]. Since they are intermediate between hollow and core@shell NPs, they have the advantages of both structures together. Indeed, their characteristic features include low density, large surface area, ease of interior core functionalization, a good molecular loading capacity in the void space, high tunability of the interstitial void space, and the presence of this hollow outer shell. Due to that, the yolk@shell NPs can therefore display enhanced properties over simple core/shell or hollow NPs in various applications [134–136]. Nonetheless, the main disadvantage comes from the difficulty to set a reproducible synthetic approach because of the complexity of their structure.

(iv) Dumbbell/Janus nanostructures: in such structures, a single NP is attached to another NP offering two functional surfaces. In this manner, the hybrid NP integrates two or more functionalities in an individual entity. Depending on the interactions at the interface, the physical and chemical properties of each component can be retained, enhanced or even weakened. Besides, the break of mirror symmetry can lead to novel effects. The successful synthesis relies on promoting heterogeneous over homogeneous nucleation processes (*i.e.* the formation of separate NPs of the second component) [137]. When Au NPs are used, these NPs can also display LSPR in a wide range of the visible spectrum [138,139]. However, the principal disadvantages are related to the lack of simple synthetic procedures and difficulties in characterizing and unambiguously verifying their formation. Moreover, the contact area between the two components is smaller than that of core@shell heterostructures precluding in most cases synergistic effects.

(v) Gold-decorated nanostructures: this structure is the result of linking a large number of small Au NPs to the surface of another NP. Frequently, negatively (or positively) charged satellite Au NPs are immobilized on a positively (or negatively) charged NP *via* electrostatic interactions or by using a bridging polymer anchored to both NPs [140,141]. Then, this route relies on surface functionalization. In this way, the distance and consequently the interaction between the two NPs can, thus, be adjusted [142]. Another strategy to obtain these heterostructures involves the *in situ* formation of Au NP seeds on the surface of NPs *via* the reduction of $HAuCl_4$ in a way that the total specific area is enhanced [143,144]. However, such heterostructure exhibits a lower contact between the NPs compared to the above mentioned ones.

(vi) Decorated gold NPs: they represent the complementary case of the previous one. Here, large Au NPs are decorated with smaller ones of different nature. In this approach, the small NPs are usually linked *via* electrostatic interactions to a previously prepared bigger Au NP. Therefore, the Au NP decoration permits to work with big Au NPs such as rods, triangles and stars. As in the core@sell nanostructure, this one also exhibits a high total specific area but a less intense contact between both NPs.

4.2. Synthesis and properties

In this section, we will review the most relevant Au-CP heterostructures, how they are synthesized and the novel or enhanced properties they exhibit, as well as the synergistic effects arising from such combinations. Additionally, the resulting properties and applications will also be discussed.

4.2.1. Au-PBA

Regarding the heterostructures formed by Au and PB/PBA, the first combinations were achieved through electrochemical deposition of PB on Au [145–148]. Nevertheless, the achieved hybrid material is deposited on an electrode as a film, limiting their applications. The first example of PB coating Au NPs was reported by Xia using colloidal chemistry [149]. In this method, the key step is the reduction of ferric ions catalyzed by Au NPs, which controlled the formation rate of PB. Later on, PB NPs decorated with Au NPs were prepared using albumina as a linker between the two components *via* the conjunction of thiolate linkages and alkylamines [150]. However, this protein coverage avoided a close contact between both systems. A similar approach was developed to prepare PB@Au core-satellite NPs, using different organic polymers as linkers and different surface functionalizations [151].

More recently, very small core@shell NPs were obtained by growing a PB shell onto a citrate-stabilized Au core [152]. Similarly, a well-rounded PB shell over Au was obtained through the initial etching of the Au core by CN^-, which provided an anchoring of these ligands around the Au surface, and the subsequent formation of the PB shell. In all these systems, the general protocol consisted of first stabilizing Au NPs with citrate and then treating these functionalized NPs with CN^- ligands (coming from the ferricyanide precursor) in order to replace the citrates with CN^- [153–155]. However, the CN^- etching complicates the use of anisotropic Au NPs because these NPs are too reactive towards cyanide [156]. Note that these protocols have been optimized to obtain Au-PB nanostructures for biomedical applications since PB is an excellent candidate as theragnostic nanomaterial [75]. In these nanostructures, Au NPs serve as practical platforms for therapeutic agents and cell imaging [6]. Thus, the Au-PB combination has resulted in the development of nanomaterials with improved biological properties such as *in vivo* computing tomography and photo-thermal therapy showing precise diagnostic guidance, significant therapeutic efficiency and high biological stability (Fig. 7a) [151,152,154,157]. A review on this topic has been recently published [54].

Moreover, recent works have integrated other PBA compounds apart from PB in the core@shell heterostructure. Thus, Marin-Pasturel et al. developed heterostructures consisting of a double shell of PBA surrounding an Au spherical core, where the core and the shell size can be modulated, therefore exhibiting different magnetic and plasmonic properties. Furthermore, they synthesized for the first time different Au@PBA@PBA' using an elegant approach based on the synthesis of cyanide-stabilized Au NPs in water through reduction of the precursor $[Au(CN)_2]^-$ with sodium borohydride followed by the sequential growth of one or more PBA shells (Fig. 8a-8d) [126,158,159]. These new hybrid NPs have also been used for biomedical applications and electrocatalysis.

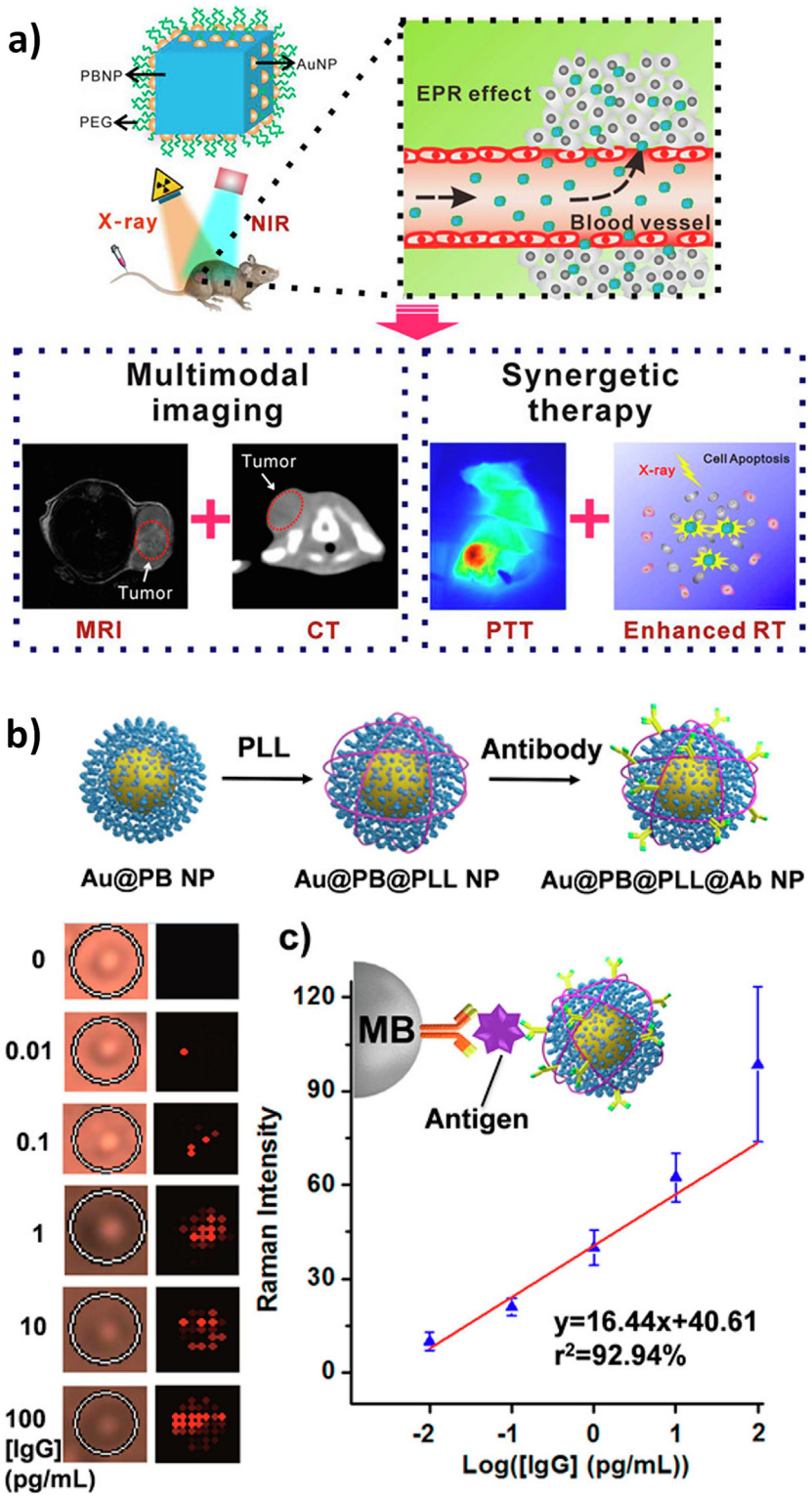

Fig. 7. Examples of Au-PB NPs used for biomedical applications. a) Development of multifunctional nanotheranostic Au decorated PB NPs. Au and PB NPs are two kinds of intrinsic theranostic nanomaterials for magnetic resonance (MR) – computed tomography (CT) imaging and synergistic photothermal and radiosensitive therapy (PTT–RT). PB as core enables T1- and T2-weighted MR contrast and strong photo-thermal effect, while Au as decorated NPs offers CT enhancement and radiosensitization. Adapted from [151]. b) Preparation of the antibody-modified Au@PB SERRS probe by coating PLL on Au@PB NPs to provide free amine moieties, which were coated with the negatively charged antibodies subsequently. Brightfield and Raman mapping (2156 cm^{-1}) of the single core@shell NPs for probing various amounts of antigen ranging from 0.01 to 100 pg/mL. All Raman mapping results were yielded under the same conditions. Adapted from [153].

Note that the synthetic routes so far developed to prepare Au-PBA nanostructures are restricted in most cases to PB and the synthesis of Au@PBA@PBA' is also limited to Au spherical cores and few PBA shells. To overcome this limitation, we have proposed a general and versatile synthetic approach to prepare hybrid Au-PBA magneto-plasmonic nanostructures formed by any PBA cubic

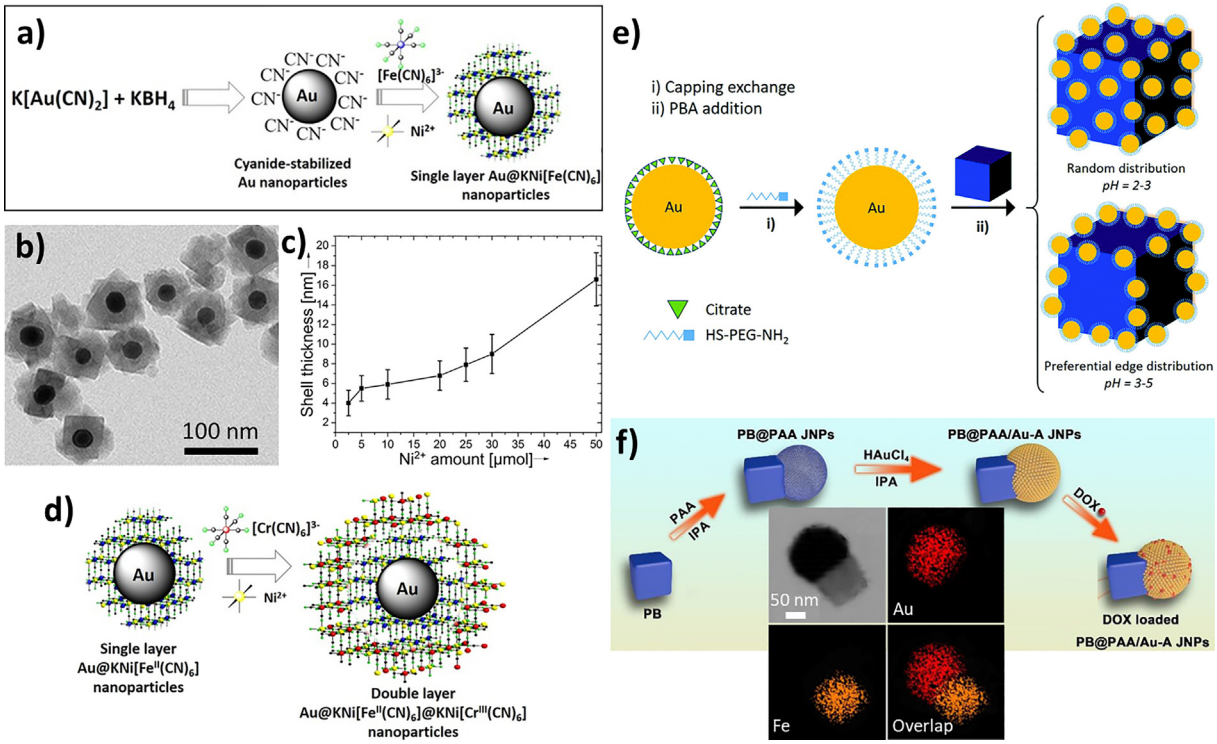

Fig. 8. Synthesis of different hybrid Au-PB/PBA nanostructures. a) Schematic representation of the approach used for the synthesis of Au@KNi[$Fe^{II}(CN)_6$] core@shell NPs. b) TEM image of Au@PBA NPs. c) Thickness of the KNi[$Fe^{II}(CN)_6$] shell *vs* the amount of Ni^{2+} added. d) Schematic representation of the synthesis of Au@KNi[$Fe^{II}(CN)_6$]@KNi[$Cr^{III}(CN)_6$] core@shell@shell NPs. Adapted from [158]. e) Schematic illustration of the preparation of heterostructures formed by Au nanospheres decorating PBA NPs. The first step involves a capping substitution and the second step corresponds to the attachment of the Au onto the PBA surface. Two different Au decorations can be achieved by adjusting the pH: a random and a preferential distribution on the edges. Adapted from [140]. f) Schematic illustration of the preparation of DOX-loaded PB@PAA/Au-A JNPs and EDAX mapping of the resulting heterostructure. Adapted from [160].

NP decorated by Au NPs of different shapes and connected to the PBA surface through a bridging molecule (Fig. 8e). Thanks to the possibility of using different plasmonic NPs, the developed protocol allows tuning the plasmon band position in the whole range of the visible spectrum which permits studying the enhancement of the magneto-optical activity coming from the PBA NP thanks to the coupling with the plasmonic properties of the Au NP [140]. Simultaneously, magneto-plasmonic core@satellite PBA@Au–Ag nanoheterostructures were also obtained by Mamontova et al. [161] by means of a post-synthetic adsorption of a bimetallic $[AuI_2AgI_2(C_6F_5)_4(OEt_2)_2]_n$ complex with ferromagnetic PBA NPs. The authors observed that the integrity of the PBA NPs was preserved during the formation of the heterostructures, but a dramatic change in the magnetic properties occurs due to the presence of ultra-small Au–Ag nanosatellite NPs. In particular, the modification of the PBA ferromagnetic properties leads to a complex spin-glass behavior. Furthermore, an improvement of the catalytic performance towards the reduction of 4-nitrophenol was reported for the same hybrid heterostructures thanks to the ability of both components of the hybrid nanostructure to effectively catalyze the reaction. Following a similar Au reduction method, PB@AuNPs@MnO_2 core@satellite NPs were recently prepared and applied for magnetic resonance imaging and enhanced antitumor therapy. In this heterostructure, PBs were decorated with ultra-small Au NPs to enhance the catalytic OH· generation for chemodynamic therapy [162].

It is worth noting that not only Au-PB/PBA core@shell and Au-decorated NPs have been designed. PB@polyacrylic acid/Au Janus NPs were prepared by a facile and mild method using a polyacrylic acid (domain as a template to grow Au NPs preferentially (Fig. 8f) [160]. The main advantages of this structure over the common core@shell rely on the exposed surfaces of PB and Au, which guarantee the maximum absorptivity of NIR light, and an appropriate space that is reserved for drug loading. Regarding the formation of more complex heterostructures, a novel strategy was reported to prepare a therapeutic agent of Au@PB yolk@shell nanocubes by the templates of Au@Ag nanocubes under mild conditions. In this case, the PB shells were obtained through the reaction of the PB precursors ($[Fe(CN)_6]^{3-}$ and Fe(III)) with the Ag shell acting as a sacrificial template to form the resulting yolk@shell Au@PB [163]. Thanks to the high surface area of these yolk@shell NPs, doxorubicin molecules are encapsulated and, by means of chemodynamic therapy, these NPs can effectively suppress tumor growth.

On the other hand, the combination of Au NP with PB/PBA can also improve the catalytic performance of pristine PB/PBA materials. For instance, core@satellite Au-PBA nanoarchitectures behave as an excellent catalyst for the reduction of 4-nitrophenol thanks to the ability of both components of the hybrid nanostructure to effectively catalyze the reaction [161]. Moreover, the conductivity increment of the resulting hybrid material can also be beneficial for some electrocatalytic reactions such as the Oxygen Evolution Reaction (OER). Indeed, recently we showed that the catalytic activities of different Au-PBA nanostructures were sharply improved thanks to the introduction of Au NPs inside a core@shell structure (Fig. 9). It was observed that the high contact between both materials gives rise to a strong synergistic effect where the Au core increases the electrochemical activity and the electrochemical stability of the PBA, while the PBA shell protects Au from its electrochemical oxidation [164]. Such improvement has similarly been reported for other electrochemical processes. Indeed, an enhancement of the electrocatalytic activity was also detected by introducing Au NPs in various PB and PBAs toward the reduction of hydrogen peroxide

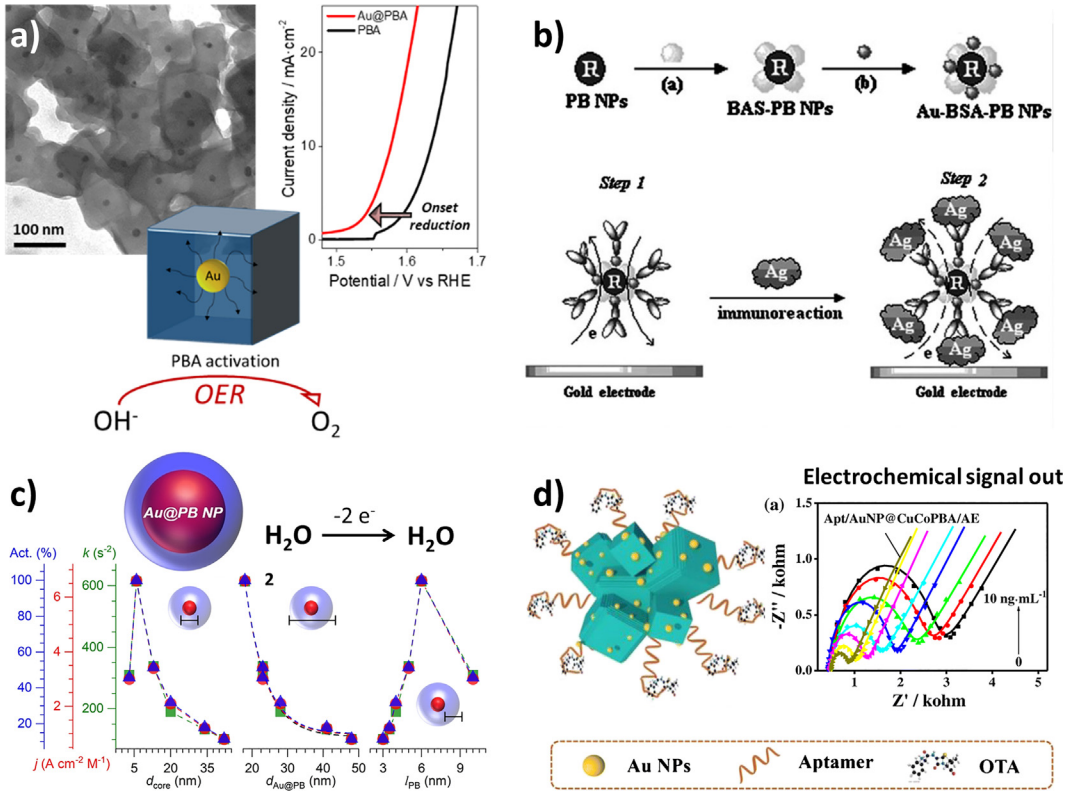

Fig. 9. Improvements in the PB/PBA electrochemical activity thanks to the introduction of Au NPs. a) Application of Au@PBA (of NiFe and CoFe) NPs for the electrochemical production of oxygen. Compared to the PBA without Au, it was found that the introduction of small amounts of Au (5–10% in weight) in the core@-shell structure gives rise to an important enhancement of the PBA activity and the overall electrochemical stability. Adapted from [164]. b) Schematic diagram of the fabrication process of Au-BSA-PB NPs and the stepwise procedure of the immunoreaction; the electron transfer pathway of the immunosensor before (step 1) and after (step 2) the immuno-interaction. Adapted from [150]. c) Electrochemical and catalytic performance as a function of Au NPs core size, Au@PB NPs size and PB thickness. Adapted from [165]. d) Application of Au-CuCoPBA nanostructures for the detection of ochratoxin a toxin by electrochemical impedance spectroscopy. Adapted from [166].

[148,149,165], toxins [166] and protein molecules such as α-1-Fetoprotein [150]. Indeed, the presence of Au increases the recorded current, which facilitates the detection of a given molecule. This leads to the improvement in the electrochemical detection/recognition of different molecules and thus to the preparation of very sensitive electrochemical sensors based on PB/PBA (Fig. 9). Interestingly, thanks to the biocompatibility of these hybrids, biosensors can be also developed [154].

In Table 2, the most relevant Au-PB/PBA heterostructures are summarized. It can be noted that the core@shell (Au@PB/PBA) is the most colloidally stable heterostructure thanks to the negatively charged surface of naked PB/PBA NPs. This property is crucial for their use in biomedical applications but it is not critical for electrocatalysis or electrosensing. Still, it is important to remark that good colloidal stability of Au and PB/PBA NPs is needed when they are combined to form a hybrid nanostructure.

4.2.2. Au-MOF

Au-MOF core@shell nanocomposites have been prepared following two main methods: (i) by encapsulation (attachment) of

Table 2
Structure, synthesis, colloidal properties and applications of known Au-PB/PBA heterostructures.

Material (structure)	Synthetic approach	Colloidal stability (size)	Application	Reference
Au@PB (core@shell)	Reduction of ferric ions around Au NPs	Colloids (30–60 nm)	Electrocatalysis of H_2O_2	[149]
PB-Au (Au decorated on PB)	Albumina as a linker between the two components	Suspension (70–100 nm)	Electrosensing of α-1-Fetoprotein Based	[150]
Au@PB (core@shell)	Au etching by CN^- and subsequent PB formation	Colloids (80 nm)	MR/SERS bimodal agents	155]
Au@PBA@PBA' (core@shell@shell)	Controlled growth around stabilized Au@CN^- NPs	Colloids (35–135, tunable)	Single-photon emission computed tomography imaging	[157,158]
Au-PBA (Au decorated on PB)	HS-PEG-NH_2 as a linker between the two components	Suspension (150 nm)	Enhancement of the MOKE effect	[140]
PB@PAA/Au-A (Janus NPs)	Polyacrylic acid as a template to preferentially grow Au	Colloids (210 nm)	Chemotherapy and photo-thermal therapy	[160]
Au@PBA (core@shell)	Controlled growth around stabilized Au@CN^- NPs	Colloids (80–90 nm)	Electrocatalysis of O_2	[164]
Au-CuCoPBA (Au decorated on PBA)	Reduction of Au salt around PBA NPs	Composite (700 nm–1 μm)	Electrosensing of ochratoxin a toxin	[165]

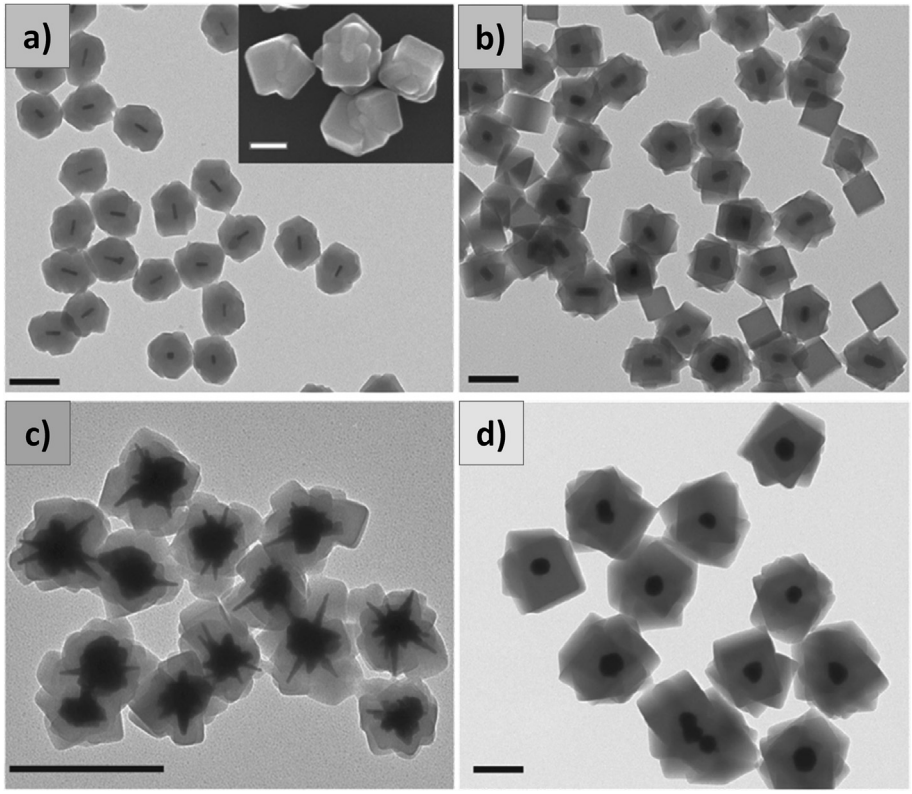

Fig. 10. Representative TEM images of different plasmonic NPs encapsulated in ZIF-8 MOF crystals: a) AuNRs, b) AuNRs@Ag core@shell, c) AuNSs, and d) spherical Au NPs. Scale bars represent 200 nm. The inset in (a) shows a detailed surface morphology of the ZIF-8 coating. Scale bar represents 100 nm. Adapted from [131].

pre-synthetized Au NPs into the pores (on the surface) of the MOF, and (ii) by direct growth of the MOF on the Au NP surface.

The first Au loading into the pores of a MOF was reported in 2005 for MOF-5 with the aim of using it in CO oxidation catalysis [167]. Further investigations reported encapsulated Au NPs in ZIF-8 [168] and MIL-101 [169]. For ZIF-8, an improvement of the catalytic activity was observed with increasing Au loadings, and the highest catalytic activity was obtained for a gold loading of 5.0 wt%. For MIL-101, Au–Pd clusters were adsorbed inside this activated MOF using a simple liquid impregnation method. However, despite the increasing endeavors to control the size, composition, dispersed nature, spatial distribution and confinement of the incorporated NPs within MOF matrices [84,170,171], the preparation of a single Au NP core coated with a uniform MOF shell remained challenging. Indeed, although the aforementioned nanocomposites exhibit a core@shell structure, they are actually composed of several Au NPs embedded in a MOF matrix rather than a single NP surrounded by a MOF shell. In fact, core@shell particles with individual cores are more difficult to synthesize because they require correct concentrations of Au and MOF precursors as well as a precise control of the reaction kinetics to avoid MOF self-nucleation [172]. In 2013, a one-pot method for the preparation of single Au NP cores coated with a uniform MOF shell of MOF-5, ZIF-8 and IRMOF-3 was established [173]. Simultaneously, Khaletskaya et al. also obtained a core@shell of Au@Al(OH)(1,4-ndc) (1,4-ndc = naphthalenedicarboxylate) composed of individual AuNR cores surrounded by a MOF shell [174]. To ensure the accurate MOF crystal nucleation onto Au rods, the Au was first coated with a hydrated amorphous alumina layer. These Al-modified rods were then used as reactive seeds in such a way that the dissolution of the alumina coating by microwave treatment in the presence of 1,4-ndc promoted the MOF nucleation specifically on the surface of the rods. Besides, in this system, a high synergistic effect between both materials was found. Just after, Hu et al. proposed a surfactant mediated method for coating single Au octahedral NPs with ZIF-8 [175]. In this work, instead of using a metal layer, cethylammonium bromide (CTAB) was added to align the overgrowth of the MOF. This turned out to be essential to induce ZIF-8 nucleation (and/or adsorption) and its further overgrowth even on anisotropic metal surfaces (Fig. 10) [131]. This new methodology (*i.e.* using other quaternary ammonium ions as surfactants, or polymers such as poly(ethylene glycol) (PEG)), allowed researchers to successfully obtain single anisotropic Au NPs coated with a uniform MOF shell. In this line, AuNRs coated by a NU-901 shell were obtained by functionalizing the Au surface with PEG to avoid the aggregation of the Au NPs prior to the MOF shell growth [23]. Other capping agents such as polyvinylpyrrolidone (PVP) have also been used to coat AuNRs, as well as for the MOF nucleation and growth [176]. As shown in these different examples, the pre-functionalization of the Au surface is crucial to colloidally stabilize the Au NPs and to permit the formation of uniform MOF shells around them. It is important to mention that in core@shell NPs, there are Au capping agent molecules between the core and the shell that lowers the physical contact and therefore the electronic interaction between the two components. This effect can be aggravated when using larger spacer molecules like PEG or PVP. In this line, Dai et al. removed by chemical treatment the PVP capping agent in an Au@MOF-808 system while maintaining the integrity of the MOF shell [177]. In particular, the removal of the capping agent was achieved following a method relying on the use of a mixture of a good solvent with a poor one, in an appropriate ratio under acidic conditions.

The synthesis of the aforementioned heterostructures reveals the importance of the fine synthetic control required for Au surface functionalization prior to the MOF growth (Fig. 11a). Furthermore, it is worth mentioning that the majority of the reported synthetic

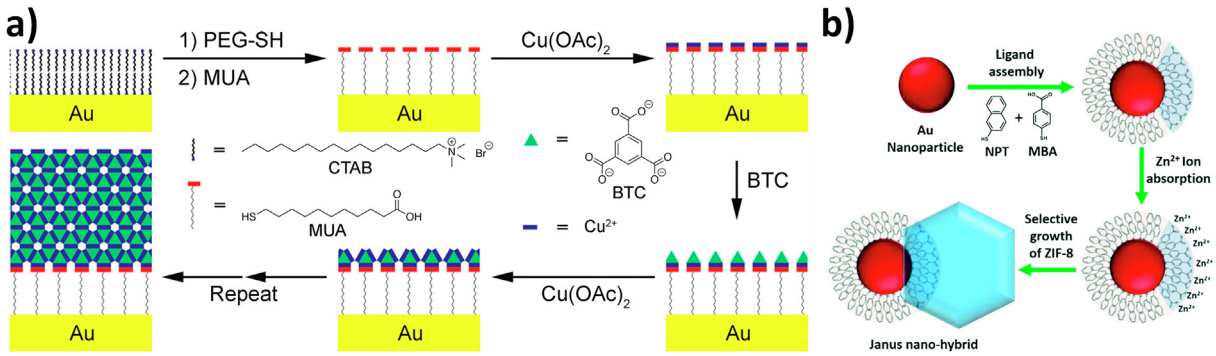

Fig. 11. Synthetic protocols for coating AuNRs and for obtaining Janus NPs. a Layer-by-Layer coating of AuNRs with HKUST-1. Adapted from [178]. b) Illustration of the ligand assembly process for the growth of Janus Au-ZIF-8 nano-hybrids. Adapted from [184].

methods for overgrowing MOF shells on metallic NPs do not permit a precise control for the shell thickness under 10 nm. In order to overcome this limitation, layer-by-layer methods have recently been used. For instance, Hinman and coworkers developed a protocol to accurately control the thickness of an HKUST-1 shell on AuNRs [178]. Nonetheless, this protocol requires consecutive centrifugation of the colloidal dispersion that may favor some aggregation. Therefore, the development of systematic, reproducible and controlled protocols to easily cover Au NPs of different morphologies with different MOFs still remains challenging.

In sharp contrast to what happens in core@shell structures, few Au@MOF yolk@shell NPs have been reported. Still, these nanostructures are more efficient as nanocarriers for loading drugs. Indeed, the design of yolk@shells provides a large hollow cavity structure with more loading space, while the shell maintains its protective character. In the meantime, the porous shell allows the guest molecules to diffuse in and out. Therefore, designing the yolk@shell nanostructures in biological research is very attractive. With this aim, yolk@shell NPs of Au@MOF have been designed for tumor diagnosis and therapy. For example, AuNSs@MOF yolk@shell that exhibit synergistic anticancer effects based on their photo-thermal and promoted cargo release properties were obtained. These particles were prepared after synthesizing the core@shell and the selective MOF etching by means of tannic acid [179]. The employed protocol is simple and might be extended to other plasmonic NPs since it involves the MOF etching and the usage of PVP as Au capping agent. Furthermore, PtAu@HKUST-1 petalous yolk@shells were successfully prepared by conversion of the corresponding PtAu@M_xO_y core@shell self-template through the oxidative dissolution of the oxide shell in a mildly acidic solution [180]. The most recently reported nanostructure is an Au@Zn/Ni-MOF-2 yolk@shell nanostructure prepared by adding all the precursors in a mixture of dimethyacetamide, dimethylformamide, ethanol, and PVP together [181]. Firstly, Au tiny particles were formed. Then, the solid Au@Zn/Ni-MOF-5 core@shell was obtained through the growth of the Zn/Ni-MOF-5 shell on PVP-functionalized Au NPs. Finally, unique hollow nanostructures were achieved by a rare crystal structure transformation from the initial solid to the Au@Zn/Ni-MOF-2 yolk@shell. It is important to remark that, although MOFs already have a remarkable free space, their preparation as heterostructures may bring an added value to enhance some targeted properties (drug delivery, catalysis, etc).

As we have reported before, most of the resulting Au-MOF composites are core@shell materials in which the metallic NP is embedded within the MOF. However, a few Janus particles formed by a single MOF and Au NPs have also been described [182–184]. For example, Janus Au- ZIF-8 nanostructures were prepared by means of a ligand-controlled approach (Fig. 11b). The selective growth is driven by the surface functionalization of Au NPs by means of competitive ligand adsorption. Hydrophilic and hydrophobic ligands are used to adsorb and assemble on Au NPs, resulting in an anisotropic surface which has different affinities to ZIF-8 precursors. In this way, it was possible to induce a break of the symmetric MOF growth around the Au NP surface. Interestingly, the ligand ratio is a key factor for manipulating the coverage of ZIF-8 on Au NPs. In addition, this synthetic protocol permits to work using anisotropic plasmonic NPs, enabling the manipulation of the resulting optical properties [184].

At the end of this section, we want to emphasize some of the benefits provided by Au in the hybrid Au-MOF nanostructure. First, Au can catalyze many different reactions and, thus, allows performing versatile coupling reactions (*i.e.* tandem reactions). Pursuing this goal, Au NPs were deposited on the surface of NH_2-UiO-66 nanocrystals in order to produce in a first step unsaturated alcohols that will then react with methylene compounds to form extended conjugated systems. In this sense, Au decorated CP materials are very promising heterostructures toward catalysis involving cascade processes [185,186]. However, as pointed out by Dai and coworkers, capping agents often lower the reactivity of the Au after being surrounded by a CP shell [177]. Therefore, attention must be paid to the capping agent removal in order to activate the catalytic reaction. In addition, the catalytic performance of plasmonic systems can be further enhanced upon light irradiation thanks to a plasmon-assisted catalytic effect [161]. This effect has been exploited to enhance the catalytic activity of different MOF shells [187–190]. In these cases, the MOF ensures the dispersity and stability of Au NPs and facilitates the mass transfer of a given molecule, while the Au generates hot electrons after plasmon excitation (Fig. 12a). In this context, Au@UiO-66 nanostructures, formed by multi-Au cores surrounded by a MOF matrix, have been used for direct photocatalytic nitrogen fixation reaction mediated by the Au NPs. In the case of yolk@shell structures, the cavity has a strong influence on the catalysis; thus, its control is crucial in order to prepare efficient "nanoreactors". In this way, this unique morphology offers several advantages in heterogeneous catalysis. For example, different activation energies for cyclohexene hydrogenation were obtained for nanostructures with and without the cavity in between the core and the shell [136]. In this regard, a PtAu@HKUST-1 nanostructure was used as a catalyst for the liquid-phase hydrogenation of olefins showing high stability and catalytic activity [180]. As aforementioned, the increment of the electrocatalytic activity thanks to the introduction of Au NPs can be used to develop electrochemical sensors of different molecules. Some hybrid Au-MOF nanomaterials have, therefore, been proposed as an electrochemical sensor of nitrobenzene [191], nitrites [192], hydroxylamine [193], gallic acid [194], and isoproturon [195].

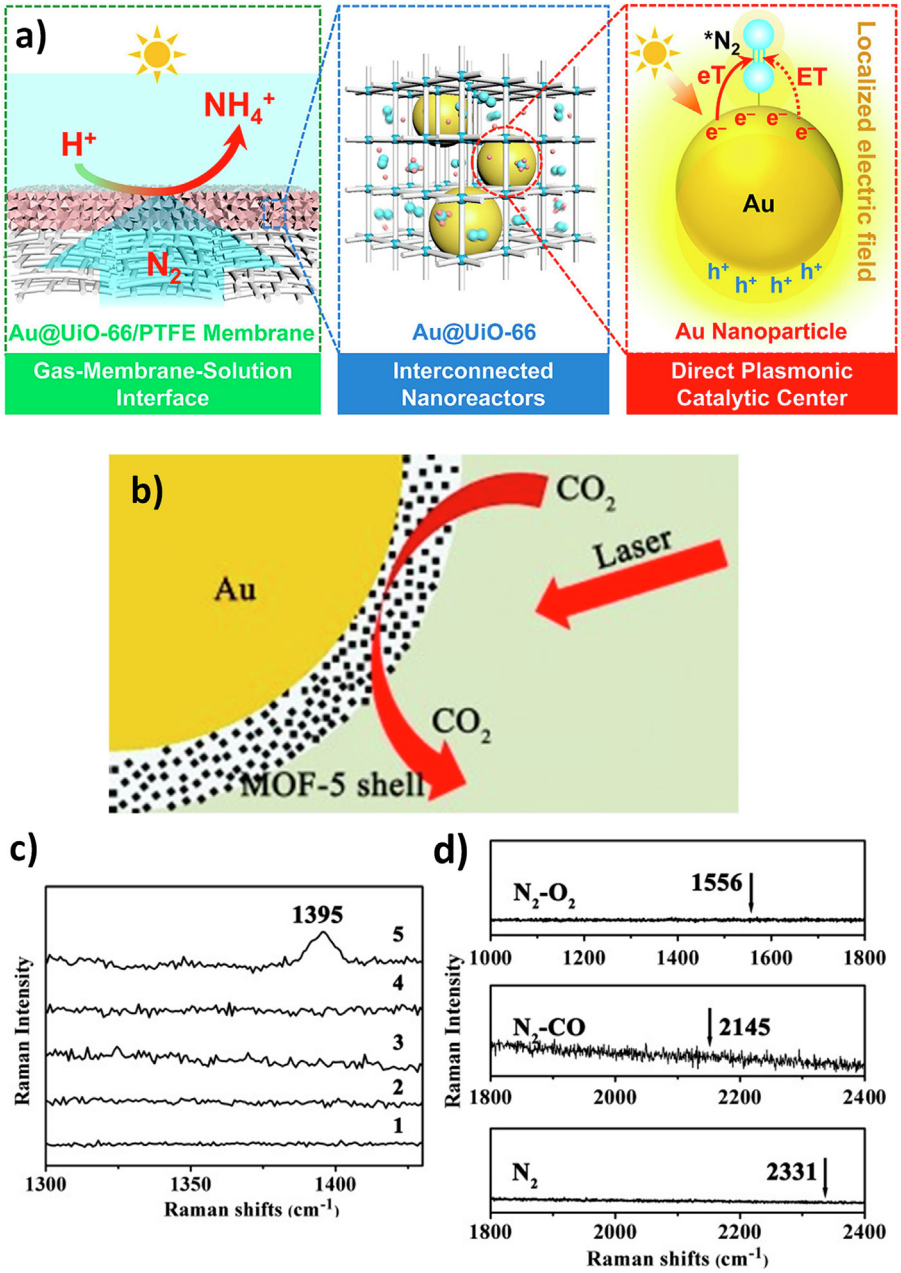

Fig. 12. Examples of the application of the plasmonic properties in catalysis and sensing. a) Schematic illustration for direct photocatalytic nitrogen fixation reaction on Au NPs encapsulated in UiO-66 matrix. The interconnected pores in the MOFs matrix facilitate the diffusion of N_2 molecules and further promote the reaction. Upon visible irradiation, the hot electrons generated on the Au NPs can be directly injected into the N_2 molecules adsorbed on Au surfaces. Such N_2 molecules can be additionally activated by the strong but evanescently localized surface plasmon resonance field, resulting in a lower apparent activation energy. Adapted from [189]. b) SERS effect on Au@MOF-5. c) SERS spectra of single Au NPs (trace 1), single MOF-5 spheres (trace 2), and Au@MOF-5 NPs with different shell thicknesses toward CO_2 in a CO_2/N_2 gas mixture. The thinnest shell (under 4 nm) is the only one active (trace 5). d) SERS spectra of single Au@MOF-5 NPs with a thinner shell toward N_2, CO, and O_2. The arrows point to the characteristic SERS peak positions of N_2, CO, and O_2. Adapted from [173].

The second example uses the photo-thermal effect of Au to control the adsorption or desorption of molecules carried by MOFs in these nanostructures [196]. Thus, the loading properties of the MOF can be used for drug delivery [174,197–199], while the use of NIR light coupled to the plasmonic absorption of the Au NP provides a molecule-release mechanism, creating local temperature gradients and, thus, the thermodiffusion of the molecule [174,199]. In this context, Au@MOFs have been proven as excellent multifunctional theragnostic nanoplatforms [200]. In addition to this, the high adsorption capability of MOFs makes the Au-MOF heterostructures highly sensitive SERS materials that can be used, for instance, for tumor marker alpha-fetoprotein in human serum [201]. Furthermore, by selecting an appropriate MOF shell, it is possible to combine the photo-induced singlet oxygen generation behavior characterized by the MOF shell with the efficient conversion of light into heat of the Au cores. Interestingly, these plasmonic properties provided by the Au NPs could also be applied for catalysis [202].

A third benefit provided by Au NPs comes from the SERS effect, which can be of interest for sensing applications. Indeed, a hybrid material can be designed for chemical sensing of high SERS signal molecules by combining the selectivity and easy adsorption of MOFs with the plasmonic effect provided by the Au NPs [201,203]. To name a few, thanks to the SERS effect, Au@MOF-5

Table 3
Structure, synthesis, colloidal properties and applications of reported Au-MOF heterostructures.

Material (structure)	Synthetic approach	Colloidal stability (size)	Application	Reference
Au@MOF-5 (Au encapsulated in MOF)	Thermal metal–organic chemical vapor deposition loading	Suspension (200 nm)	CO oxidation catalysis	[167]
Au@MOF-5 (core@shell)	Direct mixing of Au and MOF precursors	Colloids (36 nm)	Sensing of N_2, CO, and O_2	[173]
AuNRs@Al(OH)(1,4-ndc) (core@shell)	Al deposition on AuNRs and Al dissolution by microwave treatment	Suspension (100–300 nm)	Light-induced molecular release	[174]
AuNRs@HKUST-1 (core@shell)	Layer-by-Layer coating of AuNRs	Colloids (20 × 80 nm)	/	[178]
Au-ZIF-8 (Janus NPs)	MOF growth on Au NPs using competitive ligands	/(200 nm)	Catalysis of 4-nitrophenol	[184]
Au/NH_2-UiO-66 (Au decorated on MOF)	Direct mixture of the two compounds	Suspension (80 nm)	Tandem catalysis of cinnamyl alcohol	[185]
Au@UiO-66 (Au encapsulated in MOF)	Impregnation and Reduction of an Au salt on the MOF surface	Suspension (150 nm)	Photocatalytic nitrogen fixation reaction	[189]
Au/NH_2-MIL-125(Ti) (Au decorated on MOF)	Reduction of an Au salt on the MOF surface	Composite (200 nm – 1 μm)	Electrosensing of gallic acid	193]

nanohybrids were applied for the detection of CO_2 in gas mixtures (Fig. 12b) [173]. Also, Uio-66 and Uio-67 compounds with relatively large surface area and permanent high porosity were used to load and prevent the precipitation of Au NPs and thus, to permit the acquisition of excellent Raman signals of the pesticide acetamiprid [204].

Table 3 summarizes the most significant Au-MOF heterostructures. These hybrid nanomaterials can be applied in numerous fields and their colloidal stability is not always crucial. Yet, colloids are required to benefit from the plasmonic properties in SERS detection or biomedicine, and thus, colloidal chemistry emerges as a reliable method to prepare functional hybrid NPs based on Au and MOF.

4.2.3. Au-SCO

Coupling spin crossover phenomenon and plasmonic properties into a hybrid nanostructure is attracting great interest in molecular magnetism. In this regard, plasmonic properties have been mainly used for taking advantage of i) the photo-thermal plasmonic effect of Au to heat the hybrid material and induce the spin transition and ii) to detect the spin transition thanks to the high sensitivity of the plasmon.

Combinations of SCO complexes and Au NPs in hybrid heterostructures were initiated following a decoration protocol. In this context, attachment of Au NPs on the surface of [Fe(NH_2-trz)$_3$](Br) was first reported in 2008 with the purpose of evidencing the presence of the amino groups on the SCO surface [103]. Later on, the first attempt to study the synergy between both systems was described by preparing the well-known [Fe(Htrz)$_2$(trz)](BF_4) polymeric complex (Htrz = 1H-1,2,4-triazole and trz = deprotonated triazolato(−) ligand) covered by Au using thermal evaporation deposition [205]. The resulting film was analyzed and the authors confirmed the persistence of the SCO properties of the Au coated particles. In 2014, Suleimanov and coworkers obtained a hybrid to induce the SCO transition, reducing the energy needed through the photo-thermal effect arising from the LSPR [144]. In this case, [Fe(Htrz)$_2$(trz)](BF_4) was decorated with ultra-small Au NPs of ~2 nm. These Au NPs were attached to SCO NPs covered with a thin layer of silica shell that were firstly synthesized using the reverse micelle technique (Fig. 13). By exciting the nanocomposite at different laser wavelengths, a full switching was carried out and a notable photo-thermal effect was noticed. Indeed, the laser power required to complete the spin transition was reduced by around 70 % in presence of the Au NPs. The size of the Au NPs was increased to ~15 nm in order to improve this performance, but Raman spectra could not be recorded possibly because of the SERS effect associated with the larger particles. In the same year, a similar Au decoration was also used by Qiu et al., obtaining analogous nanohybrid material displaying a photo-thermal effect [143]. In this case, the Raman measurements indicated that Au NPs caused an efficient photo-thermal heating in the hybrid nanocomposites, leading to about 100 times reduction of laser energy needed for spin state switching compared with the particles without Au. Later on, in 2016, Moulet et al. went one step further and reported direct Au decoration of the [Fe(Htrz)$_2$(trz)](BF_4) without any silica shell [141]. They developed a simple protocol to anchor Au over the SCO particles by taking advantage of the Au affinity to nitrogen atoms present in the triazole ligands. Besides, they were able to tune the Au NPs size (from 4 to 45 nm) and ensure good coverage, but no photo-thermal effect was observed, maybe because of the relatively weak laser power that was applied. Then, other plasmonic metals such as Ag were also used. Thus, Li et al. decorated Ag nanowires with two NPs exhibiting spin transition: the well-known [Fe(Htrz)$_2$(trz)](BF_4) and the Hofmann clathrate [Fe(pz){Pt(CN)$_4$}] [120]. Although the nanocomposites retained their SCO properties, the electrical conductivity was unaffected by the spin transition.

Following this overview, one can conclude that even if some metal nanocomposite materials have been successfully designed, the impact coming from the metallic decoration on the physical properties does not show effective synergistic properties [120,141,143,144,205]. This limitation is very likely due to an inefficient interaction between the metal and the SCO material. To overcome this limitation, a core@shell heterostructure has shown to be more appropriate to ensure an intimate interaction between both nanosystems.

On this basis, in 2019, a simple chemical protocol was developed to prepare for the first time Au@SCO NPs based on the [Fe(Htrz)$_2$(trz)](BF_4) SCO [113]. The synthesis relies on a two-step approach consisting of a partial surface ligand substitution of the citrate-stabilized Au NPs followed by the controlled growth of a very thin layer of the SCO polymer (around 4 nm thickness) which maintains its cooperative spin transition (Fig. 14). Indeed, a large change in conductance upon spin-state switching was detected thanks to the presence of the Au core [113]. These results showed a huge improvement in the sensitivity of the device to the spin

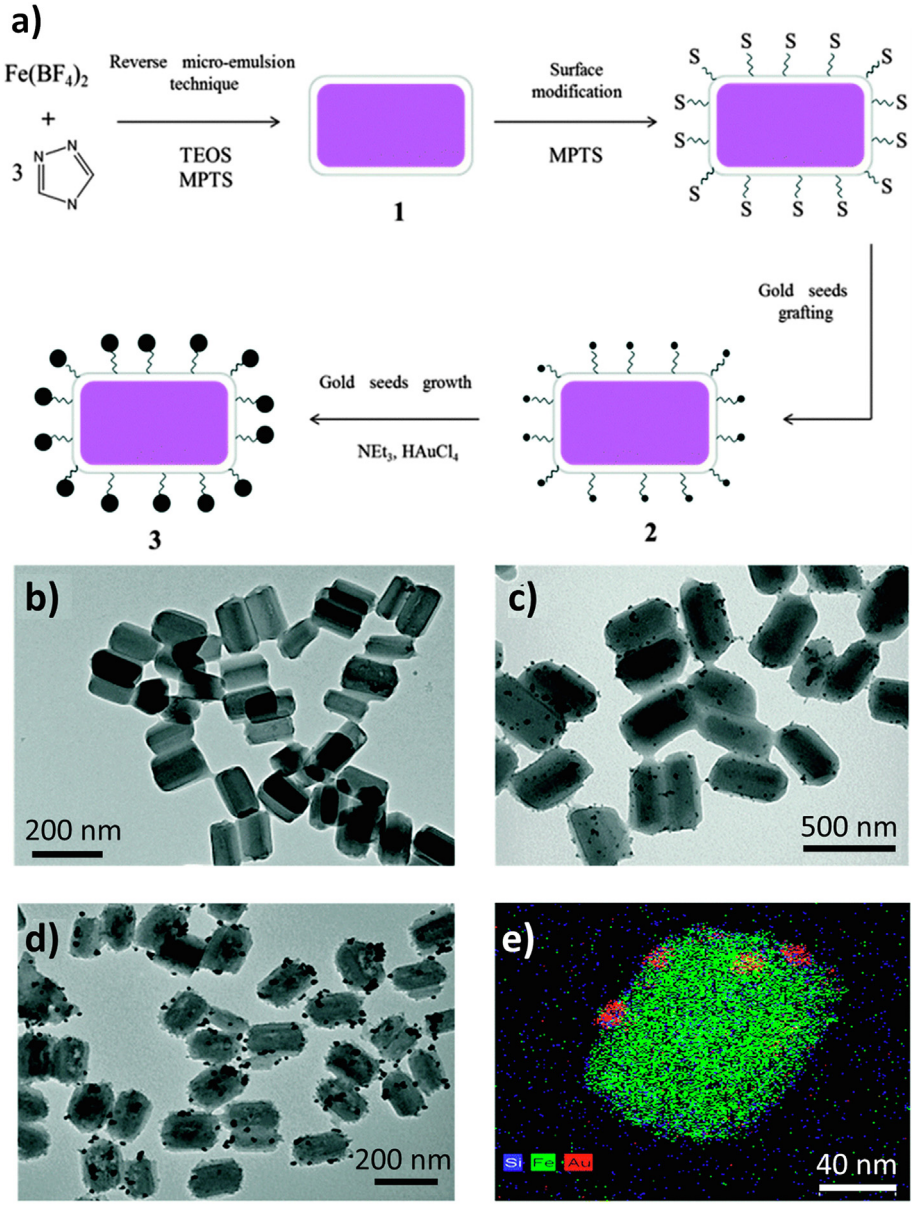

Fig. 13. Synthesis and characterization of SCO@SiO_2–Au nanocomposites a) Synthetic steps. TEM images of SCO@SiO_2 NPs (b), SCO@SiO_2 with Au seeds on the surface (c) and SCO@SiO_2–Au nanocomposites (d). e) STEM-EDX mapping of a NP from a single SCO@SiO_2–Au nanocomposite; the color code is: iron (green), silicon (blue) and gold (red). Adapted from [144]. (For interpretation of the references to color in this figure legend, the reader is referred to the web version of this article.)

transition, with values for the ON/OFF ratio, which are an order of magnitude better than the best ones obtained in previous SCO devices (Fig. 14e). In this way, the increase in the conductivity (as a consequence of the introduction of Au NP) can be used to improve the electrical detection of the spin transition.

Later on, the coverage of AuNRs by a thick $[Fe(Htrz)_2(trz)](BF_4)$ layer shell (about 65 nm along the long axis and about 40 nm along the short axis) was also undertaken by Palluel et al., leading to well-defined heterostructures [22]. The resulting nanohybrid displayed a high synergistic effect between the Au core and the SCO shell. The benefits of chemically preparing these hybrids are reflected by a strong modulation of the LSPR upon the spin transition of the SCO shell (Fig. 15) [22]. Such modulation is considerably higher than the one recorded in lithographically patterned Au nanorod arrays spin-coated by thin films of the same SCO complex [206]. In addition, the same authors investigated the effect of plasmonic heating induced by AuNRs at the single NP level [207].

Interestingly, the photo-thermal effects are enhanced in Au NPs containing hot spots as such created in the branches of AuNSs. This feature has been recently exploited in core@shell NPs formed by a metallic AuNS core and a SCO shell (Fig. 15) [130]. In this hybrid nanostructure, a photo-thermal spin transition has been observed by differential scanning calorimetry after irradiating with a very low intensity laser (much lower than the one used for the AuNRs). These synergistic effects are due to the interaction between both nanosystems, revealing the importance of the chemical design for engineering the most appropriate hybrid nanostructures.

The most important Au-SCO heterostructures are summarized in Table 4. Although the final heterostructures are not always colloidally stable, the Au or SCO particles must be well dispersed in solution during the preparation of the hybrid material, especially for the formation of core@shells. Only in this way the plasmonic properties can be properly preserved and used to switch the spin state. Then, colloidal stability is an important property to consider when synthesizing Au-SCO hybrid nanomaterials.

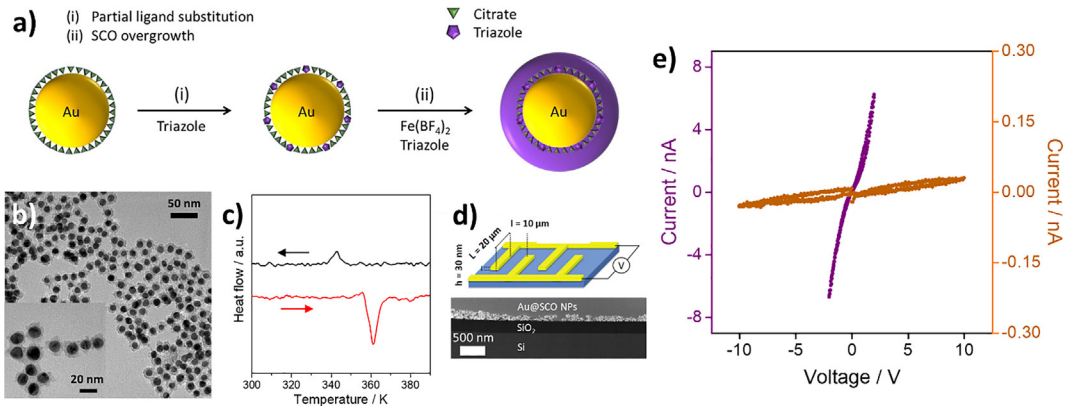

Fig. 14. Synthesis of Au@SCO core@shell NPs and electrical sensing of the spin switching. a) Schematic illustration of the steps involved in the preparation of the NPs. b) TEM image of Au@SCO NPs. Inset: HR-TEM image. c) Differential scanning calorimetry curves of Au@SCO; the red line indicates the heating mode and the black line represents the cooling mode. d) Scheme and dimensions of the Au finger-like electrode device used to measure the transport properties of an assembly of NPs (top); STEM transversal cross-section of the device (bottom). e). I–V curves of the high-conductive (purple) and low-conductive (orange) behaviors associated with the LS and HS states, respectively. Adapted from [113]. (For interpretation of the references to color in this figure legend, the reader is referred to the web version of this article.)

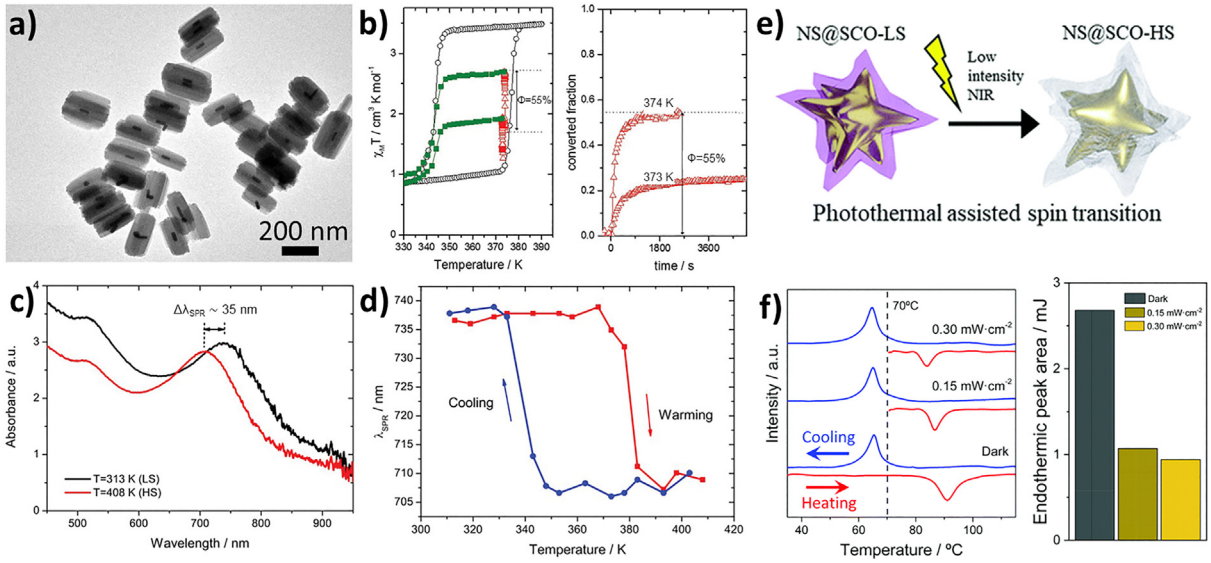

Fig. 15. Spin switching in anisotropic Au@SCO nanostructures. a) TEM image of AuNRs@SCO NPs. b) photo-switching experiments performed using a laser fluence of 15 mW·cm^{-2} centered at 830 nm. c) Optical spectra of the core@shell recorded at 313 and 408 K, respectively. d) Evolution of the peak of LSPR upon temperature variation in both warming and cooling modes. Adapted from [22]. e) Plasmon-assisted spin transition in AuNSs@SCO heterostructures. f) Differential scanning calorimetry curves of NS@SCO and variation of the endothermic area in different conditions; the red line indicates the heating mode and the blue line represents the cooling mode. Adapted from [130]. (For interpretation of the references to color in this figure legend, the reader is referred to the web version of this article.)

Table 4
Structure, synthesis, colloidal properties and applications of reported Au-SCO heterostructures.

Material (structure)	Synthetic approach	Colloidal stability (size)	Application	Reference
Au-[Fe(NH_2trz)$_3$](Br) (Au decorated on SCO)	Electrostatic interaction between both compounds	Suspension (80 nm)	Sensing of NH_2 groups	[103]
Au-[Fe(Htrz)$_2$(trz)](BF$_4$) (Au decorated on SCO@SiO_2)	Au seeds grafting and growth around SCO@SiO_2 NPs	Suspension (110 × 180 nm)	Photo-switching of the SCO state	[144]
Au-[Fe(Htrz)$_2$(trz)](BF$_4$) (Au decorated on SCO)	Surface modification of Au NPs and direct mixing with SCO NPs	Colloids (80 × 150 nm)	Photo-switching of the SCO state	[141]
Ag-[Fe(Htrz)$_2$(trz)](BF$_4$) (SCO decorated on Ag nanowires)	Controlled growth around Ag nanowires	Composite (400 nm in width)	Electrical sensing	[120]
Au@[Fe(Htrz)$_2$(trz)](BF$_4$) (core@shell)	Controlled growth around functionalized Au NPs	Colloids (20 nm)	Electrical sensing	[113]
AuNRs@[Fe(Htrz)$_2$(trz)](BF$_4$) (core@shell)	Direct addition of SCO precursor to AuNRs solution	Suspension (100 × 220 nm)	Photo-switching of the SCO state	[21]
AuNSs@[Fe(Htrz)$_2$(trz)](BF$_4$) (core@shell)	Controlled growth around functionalized Au NPs	Suspension (100 nm)	Photo-switching of the SCO state	[130]

5. Conclusions and perspectives

This review has focused on hybrid nanostructures integrating gold nanoparticles with functional coordination polymers. Gold nanoparticles have been used especially because of their unique physical properties (plasmonic properties responsible for SERS detection, photo-thermal effect and/or plasmon sensibility, and electrical conductivity, which can facilitate the conducting properties in the hybrid nanomaterial) and the possibility to use colloidal chemistry routes for designing the appropriate hybrid nanostructures targeting given functions. In their turn, coordination polymers are materials that can possess potential advantages over conventional inorganic nanomaterials and organic compounds such as structural and chemical versatility, easy processability, high specific area, good solubility, low toxicity, biodegradability and electronic and magnetic functionalities. Thus, a wise integration of Au NPs in CPs in different types of nanostructures has allowed to extend the scope of properties and applications of these CPs, overcoming some of the limitations of Au NPs for specific applications. In this regard, these hybrid materials have become promising nanostructures for applications in biomedicine, catalysis, magnetism and sensing.

In biomedical applications, the poor NIR photo-thermal therapy performance of spherical small Au NPs (that are reported as the most biocompatible plasmonic NPs) is significantly improved when combined with CPs (that may exhibit tunable optical properties). On the other hand, the photo-thermal effect of Au NPs can facilitate the adsorption or desorption of molecules carried by these hybrid nanostructures. Thanks to that, their combination with the high surface area of CPs can result in interesting usages for drug delivery.

In catalysis, the elaboration of Au-CP nanostructures paves the way for the catalysis of cascade processes and tandem reactions. Moreover, Au can also improve the catalytic performance of pristine CP materials thanks to its high electrical conductivity (for electrocatalysis), or thanks to the plasmon (for photocatalysis).

In molecular magnetism, Au plasmons have been proven as an excellent tool for inducing the spin transition in spin crossover complexes by photo-thermal effects and for electrically detecting and manipulating the spin state switching, thus facilitating its integration in molecular electronic and spintronic devices. On the other hand, a promising perspective, which merits to be further investigated, is that of combining in a single structure Au NPs with magnets based on CPs (PBA networks, for example) in order to get magneto-plasmonic effects, or even more complex phenomena arising from the photo-magnetic properties exhibited by some of these magnets.

For sensing applications, the combination of the high surface area of CPs with the plasmonic effect of Au NPs has shown to be useful for SERS sensing. In addition, the enhancement of the CP electrocatalytic activity, obtained by incorporating Au NPs, can improve the electrochemical detection/recognition of different molecules. In this line, the increase in the conductivity of the CP can also be used to improve the electrical detection of the spin transition.

Along this review, particular attention has been paid to the core@shell nanostructure made of an Au core and a functional CP shell since it maximizes the interaction between the two nanosystems, thus favoring the appearance of synergistic effects. Decorated NPs are also quite common nanostructures due to their simplicity, versatility and easy preparation. For the other possible nanostructures, the field is much less explored. Thus, few Janus and elaborated core@shell nanostructures, as the yolk@shell ones, have been reported so far, despite their recent considerable interest [133]. Moreover, the choice of CP has also been limited to very well-known CPs, as for example bimetallic cyanide complexes of the Prussian Blue family, some archetypical MOFs, or spin-crossover complexes. Indeed, there is still plenty of room available to develop new synthetic protocols, to incorporate other less-common CPs to produce novel hybrid nanomaterials and to explore different physico-chemical properties coexisting or emerging in these smart and multifunctional nanostructures.

Data availability

No data was used for the research described in the article.

Declaration of Competing Interest

The authors declare that they have no known competing financial interests or personal relationships that could have appeared to influence the work reported in this paper.

Acknowledgments

This study forms part of the Advanced Materials program and was supported by the Spanish MCIN with funding from European Union NextGenerationEU (PRTR-C17.I1) and by Generalitat Valenciana. We acknowledge funding from the EU (ERC Advanced Grant Mol-2D 788222), the Spanish MCIN (Unit of Excellence "Maria de Maeztu" CEX2019-000919-M and Project 2D-HETEROS PID2020-117152RB-100, co-financed by FEDER) and the Generalitat Valenciana (Prometeo Programme PROMETEO/2017/066, iDiFEDER/2018/061 and iDiFEDER/2020/063). R. S.-G. thanks the Spanish Ministry of Universities and the European Union for a 'Margarita Salas' postdoctoral fellowship (Next Generation EU). M. C.-P. thanks the Spanish Ministry of Universities for an International Attraction of Talent Maria Zambrano Grant.

References

[1] C. de Mello Donegá, Synthesis and properties of colloidal heteronanocrystals, Chem. Soc. Rev. 40 (2011) 1512–1546.
[2] T. Hueckel, G.M. Hocky, S. Sacanna, Total synthesis of colloidal matter, Nat. Rev. Mater. 6 (2021) 1053–1069.
[3] R. Costi, A.E. Saunders, U. Banin, Colloidal hybrid nanostructures: a new type of functional materials, Angew. Chem. Int. Ed. 49 (2010) 4878–4897.
[4] K.C.F. Leung, S. Xuan, X. Zhu, D. Wang, C.P. Chak, S.F. Lee, W.K.W. Ho, B.C.T. Chung, Gold and iron oxide hybrid nanocomposite materials, Chem. Soc. Rev. 41 (2012) 1911–1928.
[5] T.T. Nguyen, F. Mammeri, S. Ammar, Iron oxide and gold based magneto-plasmonic nanostructures for medical applications: A review, Nanomaterials 8 (2018) 149.
[6] Y.C. Yeh, B. Creran, V.M. Rotello, Gold nanoparticles: Preparation, properties, and applications in bionanotechnology, Nanoscale 4 (2012) 1871–1880.
[7] H. Jans, Q. Huo, Gold nanoparticle-enabled biological and chemical detection and analysis, Chem. Soc. Rev. 41 (2012) 2849–2866.
[8] C. Quintana, M.P. Cifuentes, M.G. Humphrey, Transition metal complex/gold nanoparticle hybrid materials, Chem. Soc. Rev. 49 (2020) 2316–2341.
[9] E.J. Devid, P.N. Martinho, M.V. Kamalakar, I. Šalitroš, Ú. Prendergast, J.F. Dayen, V. Meded, T. Lemma, R. González-Prieto, F. Evers, T.E. Keyes, M. Ruben, B. Doudin, S.J. Van Der Molen, Spin transition in arrays of gold nanoparticles and spin crossover molecules, ACS Nano 9 (2015) 4496–4507.
[10] F. Dumur, E. Dumas, C.R. Mayer, Functionalization of gold nanoparticles by inorganic entities, Nanomaterials 10 (2020) 548.
[11] G. Nasr, A. Guerlin, F. Dumur, S.A. Baudron, E. Dumas, F. Miomandre, G. Clavier, M. Sliwa, C.R. Mayer, Dithiolate-appended iridium(III) complex with dual functions of reducing and capping agent for the design of small-sized gold nanoparticles, J. Am. Chem. Soc. 133 (2011) 6501–6504.
[12] V.G. Vegas, M. Villar-Alonso, C.J. Gómez-García, F. Zamora, P. Amo-Ochoa, Direct formation of sub-micron and nanoparticles of a bioinspired coordination polymer based on copper with adenine, Polymers 9 (2017) 565.
[13] M. Faraday, Experimental relations o f gold (and other metals) to light, Philos. Trans. R. Soc. 147 (1857) 145–181.
[14] D.M.P. Mingos, Gold Clusters, Colloids and Nanoparticles I, Springer, US, 2014.
[15] G. Mie, Beitrage zur Optik truber Medien, spexiell kolloidaler Metallosungen, Ann. Phys. 3 (1908) 377–445.
[16] R. Gans, Über die Form ultramikroskopischer Goldteilchen, Ann. Phys. 342 (1912) 881–900.
[17] K.M. Mayer, J.H. Hafner, Localized surface plasmon resonance sensors, Chem. Rev. 111 (2011) 3828–3857.

[18] G. Armelles, A. Cebollada, A. García-Martín, M.U. González, Magnetoplasmonics: magnetoplasmonics: combining magnetic and plasmonic functionalities, Adv. Opt. Mater. 1 (2013) 10–35.
[19] E. Petryayeva, U.J. Krull, Localized surface plasmon resonance: Nanostructures, bioassays and biosensing-A review, Anal. Chim. Acta. 706 (2011) 8–24.
[20] K.S. Lee, M.A. El-Sayed, Gold and silver nanoparticles in sensing and imaging: Sensitivity of plasmon response to size, shape, and metal composition, J. Phys. Chem. B. 110 (2006) 19220–19225.
[21] C.L. Nehl, J.H. Hafner, Shape-dependent plasmon resonances of gold nanoparticles, J. Mater. Chem. 18 (2008) 2415–2419.
[22] M. Palluel, N.M. Tran, N. Daro, S. Buffière, S. Mornet, E. Freysz, G. Chastanet, The interplay between surface plasmon resonance and switching properties in gold@spin crossover nanocomposites, Adv. Funct. Mater. 30 (2020) 2000447.
[23] J.W.M. Osterrieth, D. Wright, H. Noh, C.W. Kung, D. Vulpe, A. Li, J.E. Park, R.P. Van Duyne, P.Z. Moghadam, J.J. Baumberg, O.K. Farha, D. Fairen-Jimenez, Core-shell gold nanorod@zirconium-based metal-organic framework composites as in situ size-selective raman probes, J. Am. Chem. Soc. 141 (2019) 3893–3900.
[24] K.A. Willets, R.P. Van Duyne, Localized surface plasmon resonance spectroscopy and sensing, Annu. Rev. Phys. Chem. 58 (2007) 267–297.
[25] E.C. Dreaden, A.M. Alkilany, X. Huang, C.J. Murphy, M.A. El-Sayed, The golden age: Gold nanoparticles for biomedicine, Chem. Soc. Rev. 41 (2012) 2740–2779.
[26] N. Tepale, V.A. Fern, C. Carreon-alvarez, V.J. Gonz, A. Luna-flores, A. Carreon-alvarez, J. Aguilar, Nanoengineering of gold nanoparticles, Crystals 9 (2019) 612.
[27] M.C. Daniel, D. Astruc, Gold nanoparticles: assembly, supramolecular chemistry, quantum-size-related properties, and applications toward biology, catalysis, and nanotechnology, Chem. Rev. 104 (2004) 293–346.
[28] E. Boisselier, D. Astruc, Gold nanoparticles in nanomedicine: preparations, imaging, diagnostics, therapies and toxicity, Chem. Soc. Rev. 38 (2009) 1759–1782.
[29] A. Corma, H. Garci, Supported gold nanoparticles as catalysts for organic reactions, Chem. Soc. Rev. 37 (2008) 2096–2126.
[30] X. Zhou, W. Xu, G. Liu, D. Panda, P. Chen, Size-dependent catalytic activity and dynamics of gold nanoparticles at the single-molecule level, J. Am. Chem. Soc. 132 (2010) 138–146.
[31] S. Guo, E. Wang, Synthesis and electrochemical applications of gold nanoparticles, Anal. Chim. Acta. 598 (2007) 181–192.
[32] L. Dykman, N. Khlebtsov, Gold nanoparticles in biomedical applications: recent advances and perspectives, Chem. Soc. Rev. 41 (2012) 2256–2282.
[33] S. Vial, R.L. Reis, J.M. Oliveira, Recent advances using gold nanoparticles as a promising multimodal tool for tissue engineering and regenerative medicine, Curr. Opin. Solid State Mater. Sci. 21 (2017) 92–112.
[34] M. Grzelczak, J. Pérez-Juste, P. Mulvaney, L.M. Liz-Marzán, Shape control in gold nanoparticle synthesis, Chem. Soc. Rev. 37 (2008) 1783.
[35] S. Barbosa, A. Agrawal, L. Rodríguez-Lorenzo, I. Pastoriza-Santos, R.A. Alvarez-Puebla, A. Kornowski, H. Weller, L.M. Liz-Marzán, Tuning size and sensing properties in colloidal gold nanostars, Langmuir 26 (2010) 14943–14950.
[36] R. Sardar, J.S. Shumaker-Parry, Spectroscopic and microscopic investigation of gold nanoparticle formation: Ligand and temperature effects on rate and particle size, J. Am. Chem. Soc. 133 (2011) 8179–8190.
[37] C.J. Ackerson, P.D. Jadzinsky, R.D. Kornberg, Thiolate ligands for synthesis of water-soluble gold clusters, J. Am. Chem. Soc. 127 (2005) 6550–6551.
[38] I. Hussain, S. Graham, Z. Wang, B. Tan, D.C. Sherrington, S.P. Rannard, A.I. Cooper, M. Brust, Size-controlled synthesis of near-monodisperse gold nanoparticles in the 1–4 nm range using polymeric stabilizers, J. Am. Chem. Soc. 127 (2005) 16398–16399.
[39] J. Turkevich, P.C. Stevenson, J. Hillier, A study of the nucleation and growth processes in the synthesis of colloidal gold, Discuss. Faraday Soc. 11 (1951) 55–75.
[40] G. Frens, Controlled nucleation for the regulation of the particle size in monodisperse gold suspensions, Nat. Phys. Sci. 241 (1973) 20–22.
[41] H. Masuda, H. Tanaka, N. Baba, Preparation of porous material by replacing microstructure of anodic alumina film with metal, Chem. Lett. 19 (1990) 621–622.
[42] C.R. Martin, Template synthesis of polymeric and metal microtubules, Adv. Mater. 3 (1991) 457–459.
[43] B. Nikoobakht, M.A. El-Sayed, Preparation and growth mechanism of gold nanorods (NRs) using seed-mediated growth method, Chem. Mater. 15 (2003) 1957–1962.
[44] N.R. Jana, L. Gearheart, C.J. Murphy, Seed-mediated growth approach for shape-controlled synthesis of spheroidal and rod-like gold nanoparticles using a surfactant template, Adv. Mater. 13 (2001) 1389–1393.
[45] N.D. Burrows, A.M. Vartanian, N.S. Abadeer, E.M. Grzincic, L.M. Jacob, W. Lin, J. Li, J.M. Dennison, J.G. Hinman, C.J. Murphy, Anisotropic nanoparticles and anisotropic surface chemistry, J. Phys. Chem. Lett. 7 (2016) 632–641.
[46] H.L. Wu, C.H. Chen, M.H. Huang, Seed-mediated synthesis of branched gold nanocrystals derived from the side growth of pentagonal bipyramids and the formation of gold nanostars, Chem. Mater. 21 (2009) 110–114.
[47] M. Iqbal, G. Usanase, K. Oulmi, F. Aberkane, T. Bendaikha, H. Fessi, N. Zine, G. Agusti, E.-S. Errachid, A. Elaissari, Preparation of gold nanoparticles and determination of their particles size via different methods, Mater. Res. Bull. 79 (2016) 97–104.
[48] D.K. Smith, B.A. Korgel, The importance of the CTAB surfactant on the colloidal seed-mediated synthesis of gold nanorods, Langmuir 24 (2008) 644–649.
[49] B.F. Hoskins, R. Robson, Design and construction of a new class of scaffolding-like materials comprising infinite polymeric frameworks of 3D-linked molecular rods. A reappraisal of the Zn(CN)2 and Cd(CN)2 structures and the synthesis and structure of the diamond-related framework, J. Am. Chem. Soc. 112 (1990) 1546–1554.
[50] R. Robson, B.F. Abrahams, S.R. Batten, R.W. Gable, B.F. Hoskins, J. Liu, Crystal engineering of novel materials composed of infinite two- and three-dimensional frameworks, Supramol. Archit. (1992) 256–273.
[51] X.M. Chen, Assembly chemistry of coordination polymers, Mod. Inorg. Synth. Chem. (2011) 207–225.
[52] G.I. Dzhardimalieva, I.E. Uflyand, Design and synthesis of coordination polymers with chelated units and their application in nanomaterials science, RSC Adv. 7 (2017) 42242–42288.
[53] S.R. Batten, S.M. Neville, D.R. Turner, Coordination Polymers: Design, Analysis and Application, Royal Society of Chemistry, 2009.
[54] L. Catala, T. Mallah, Nanoparticles of Prussian blue analogs and related coordination polymers: from information storage to biomedical applications, Coord. Chem. Rev. 346 (2017) 32–61.
[55] M. Verdaguer, G.S. Girolami, Magnetic Prussian Blue analogues, Magn. Mol. Mater. V (2005) 283–346.
[56] A. Simonov, T. De Baerdemaeker, H.L.B. Boström, M.L. Ríos Gómez, H.J. Gray, D. Chernyshov, A. Bosak, H.B. Bürgi, A.L. Goodwin, Hidden diversity of vacancy networks in Prussian blue analogues, Nature 578 (2020) 256–260.
[57] A. Paolella, C. Faure, V. Timoshevskii, S. Marras, G. Bertoni, A. Guerfi, A. Vijh, M. Armand, K. Zaghib, A review on hexacyanoferrate-based materials for energy storage and smart windows: Challenges and perspectives, J. Mater. Chem. A 5 (2017) 18919–18932.
[58] M. Evangelisti, E. Manuel, M. Affronte, M. Okubo, C. Train, M. Verdaguer, Vacancy-driven magnetocaloric effect in Prussian blue analogues, J. Magn. Magn. Mater. 316 (2007) 569–571.
[59] Z.Y. Yu, Y. Duan, J.D. Liu, Y. Chen, X.K. Liu, W. Liu, T. Ma, Y. Li, X.S. Zheng, T. Yao, M.R. Gao, J.F. Zhu, B.J. Ye, S.H. Yu, Unconventional CN vacancies suppress iron-leaching in Prussian blue analogue pre-catalyst for boosted oxygen evolution catalysis, Nat. Commun. 10 (2019) 2799.
[60] V. Escax, A. Bleuzen, C. Cartier dit Moulin, F. Villain, A. Goujon, F. Varret, M. Verdaguer, Photoinduced ferrimagnetic systems in Prussian blue analogues CIxCo4[Fe(CN)6]y (CI = alkali cation) 3. Control of the photo- and thermally induced electron transfer by the [Fe(CN)6] vacancies in cesium derivatives, J. Am. Chem. Soc. 123 (2001) 12536–12543.
[61] T. Mallah, S. Thiébaut, M. Verdaguer, P. Veillet, High-Tc molecular-based magnets: ferrimagnetic mixed-valence chromium (III)-chromium (II) cyanides with T c at 240 and 190 Kelvin, Science 262 (1993) 1554–1557.
[62] S. Ferlay, T. Mallah, R. Ouahès, P. Veillet, M. Verdaguer, A room-temperature organometallic magnet based on Prussian Blue, Nature 378 (1995) 701–703.
[63] R. Garde, F. Villain, M. Verdaguer, Molecule-based room-temperature magnets: Catalytic role of V(III) in the synthesis of vanadium-chromium Prussian blue analogues, J. Am. Chem. Soc. 124 (2002) 10531–10538.
[64] L. Han, P. Tang, Á. Reyes-Carmona, B. Rodríguez-García, M. Torréns, J.R. Morante, J. Arbiol, J.R. Galan-Mascaros, Enhanced activity and acid pH stability of Prussian blue-type oxygen evolution electrocatalysts processed by chemical etching, J. Am. Chem. Soc. 138 (2016) 16037–16045.
[65] L.M. Cao, D. Lu, D.C. Zhong, T.B. Lu, Prussian blue analogues and their derived nanomaterials for electrocatalytic water splitting, Coord. Chem. Rev. 407 (2020).
[66] L. Catala, D. Brinzei, Y. Prado, A. Gloter, O. Stéphan, G. Rogez, T. Mallah, Core-multishell magnetic coordination nanoparticles: Toward multifunctionality on the nanoscale, Angew. Chem. Int. Ed. 48 (2009) 183–187.
[67] K. Zhang, M. Tu, W. Gao, X. Cai, F. Song, Z. Chen, Q. Zhang, J. Wang, C. Jin, J. Shi, X. Yang, Y. Zhu, W. Gu, B. Hu, Y. Zheng, H. Zhang, M. Tian, Hollow Prussian Blue nanozymes drive neuroprotection against ischemic stroke via attenuating oxidative stress, counteracting inflammation, and suppressing cell apoptosis, Nano Lett. 19 (2019) 2812–2823.
[68] M. Fitta, H. Prima-Garcia, P. Czaja, T. Korzeniak, M. Krupiński, M. Wojtyniak, M. Bałanda, Magnetic and magneto-optical properties of nickel hexacyanoferrate/chromate thin films, RSC Adv. 7 (2017) 1382–1386.
[69] P. Zhou, D. Xue, H. Luo, X. Chen, Fabrication, structure, and magnetic properties of highly ordered Prussian blue nanowire arrays, Nano Lett. 2 (2002) 845–847.
[70] A.C. Felts, A. Slimani, J.M. Cain, M.J. Andrus, A.R. Ahir, K. Abboud, M.W. Meisel, K. Boukheddaden, D.R. Talham, Control of the speed of a light-induced spin transition through mesoscale core-shell architecture, J. Am. Chem. Soc. 140 (2018) 5814–5824.
[71] Y. Guari, M. Cahu, G. Félix, S. Sene, J. Long, J. Chopineau, J. Devoisselle, J. Larionova, Nanoheterostructures based on nanosized Prussian blue and its analogues: design, properties and applications, Coord. Chem. Rev. 461 (2022).
[72] M. Morant-Giner, R. Sanchis-Gual, J. Romero, A. Alberola, L. García-Cruz, S. Agouram, M. Galbiati, N.M. Padial, J.C. Waerenborgh, C. Martí-Gastaldo, S. Tatay, A. Forment-Aliaga, E. Coronado, Prussian Blue@MoS2Layer composites as highly efficient cathodes for sodium- and potassium-ion batteries, Adv. Funct. Mater. 28 (2018) 1706125.
[73] Z. Qin, Y. Li, N. Gu, Progress in applications of Prussian blue nanoparticles in biomedicine, Adv. Healthc. Mater. 7 (2018) 1800347.

[74] X. Ma, J. Hao, J. Wu, Y. Li, X. Cai, Y. Zheng, Prussian Blue nanozyme as a pyroptosis inhibitor alleviates neurodegeneration, Adv. Mater. (2022) 2106723.
[75] L. Fétiveau, G. Paul, A. Nicolas-Boluda, J. Volatron, R. George, S. Laurent, R. Muller, L. Sancey, P. Mejanelle, A. Gloter, F. Gazeau, L. Catala, Tailored ultra-small Prussian blue-based nanoparticles for MRI imaging and combined photothermal/photoacoustic theranostics, Chem. Commun. 55 (2019) 14844–14847.
[76] H. Furukawa, K.E. Cordova, M. O'Keeffe, O.M. Yaghi, The chemistry and applications of metal-organic frameworks, Science. 341 (2013) 1230444.
[77] N. Stock, S. Biswas, Synthesis of metal-organic frameworks (MOFs): Routes to various MOF topologies, morphologies, and composites, Chem. Rev. 112 (2012) 933–969.
[78] H.C. Zhou, J.R. Long, O.M. Yaghi, Introduction to metal-organic frameworks, Chem. Rev. 112 (2012) 673–674.
[79] A.E. Baumann, D.A. Burns, B. Liu, V.S. Thoi, Metal-organic framework functionalization and design strategies for advanced electrochemical energy storage devices, Commun. Chem. 2 (2019) 86.
[80] B.M. Connolly, D.G. Madden, A.E.H. Wheatley, D. Fairen-Jimenez, Shaping the future of fuel: monolithic metal-organic frameworks for high-density gas storage, J. Am. Chem. Soc. 142 (2020) 8541–8549.
[81] V. Rubio-Giménez, S. Tatay, C. Martí-Gastaldo, Electrical conductivity and magnetic bistability in metal-organic frameworks and coordination polymers: Charge transport and spin crossover at the nanoscale, Chem. Soc. Rev. 49 (2020) 5601–5638.
[82] Ü. Anik, S. Timur, Z. Dursun, Metal organic frameworks in electrochemical and optical sensing platforms: a review, Microchim. Acta 186 (2019) 18–24.
[83] K. Caamaño, R. Heras-Mozos, J. Calbo, J.C. Díaz, J.C. Waerenborgh, B.J.C. Vieira, P. Hernández-Muñoz, R. Gavara, M. Giménez-Marqués, Exploiting the redox activity of MIL-100 (Fe) carrier enables prolonged carvacrol antimicrobial activity, ACS Appl. Mater. Interfaces 14 (2022) 10758–10768.
[84] G. Lu, S. Li, Z. Guo, O.K. Farha, B.G. Hauser, X. Qi, Y. Wang, X. Wang, S. Han, X. Liu, J.S. Duchene, H. Zhang, Q. Zhang, X. Chen, J. Ma, S.C.J. Loo, W.D. Wei, Y. Yang, J.T. Hupp, F. Huo, Imparting functionality to a metal-organic framework material by controlled nanoparticle encapsulation, Nat. Chem. 4 (2012) 310–316.
[85] Y. Ye, W. Guo, L. Wang, Z. Li, Z. Song, J. Chen, Z. Zhang, S. Xiang, B. Chen, Straightforward loading of imidazole molecules into metal-organic framework for high proton conduction, J. Am. Chem. Soc. 139 (2017) 15604–15607.
[86] K. Kumagai, T. Uematsu, T. Torimoto, S. Kuwabata, Direct surface modification of semiconductor quantum dots with metal-organic frameworks, CrystEngComm 21 (2019) 5568–5577.
[87] R. Canioni, C. Roch-Marchal, F. Sécheresse, P. Horcajada, C. Serre, M. Hardi-Dan, G. Férey, J.M. Grenèche, F. Lefebvre, J.S. Chang, Y.K. Hwang, O. Lebedev, S. Turner, G. Van Tendeloo, Stable polyoxometalate insertion within the mesoporous metal organic framework MIL-100(Fe), J. Mater. Chem. 21 (2011) 1226–1233.
[88] S. Dai, A. Tissot, C. Serre, Recent progresses in metal-organic frameworks based core–shell composites, Adv. Energy Mater. 12 (2022) 2100061.
[89] A. Bousseksou, G. Molnár, L. Salmon, W. Nicolazzi, Molecular spin crossover phenomenon: Recent achievements and prospects, Chem. Soc. Rev. 40 (2011) 3313–3335.
[90] O. Kahn, J. Kröber, C. Jay, Spin transition molecular materials for displays and data recording, Adv. Mater. 4 (1992) 718–728.
[91] O. Kahn, Spin-crossover molecular materials, Curr. Opin. Solid State Mater. Sci. 1 (1996) 547–554.
[92] R.W. Hogue, S. Singh, S. Brooker, Spin crossover in discrete polynuclear iron (II) complexes, Chem. Soc. Rev. 47 (2018) 7303–7338.
[93] F. Prins, M. Monrabal-Capilla, E.A. Osorio, E. Coronado, H.S.J. Van Der Zant, Room-temperature electrical addressing of a bistable spin-crossover molecular system, Adv. Mater. 23 (2011) 1545–1549.
[94] E. Pinilla-Cienfuegos, J. Parra, A. Brimont, I. Olivares, R. Sanchis-Gual, R. Torres-Cavanillas, P. Sanchis, New molecular-based materials for enabling electro-optical bistability in the silicon photonics platform, 21st International Conference on Transparent Optical Networks, (ICTON) (2019) 1–3, https://doi.org/10.1109/ICTON.2019.8840509.
[95] G. Molnár, L. Salmon, W. Nicolazzi, F. Terki, A. Bousseksou, Emerging properties and applications of spin crossover nanomaterials, J. Mater. Chem. C 2 (2014) 1360–1366.
[96] E. Coronado, M. Giménez-Marqués, G. Mínguez Espallargas, F. Rey, I.J. Vitórica-Yrezábal, Spin-crossover modification through selective CO2 sorption, J. Am. Chem. Soc. 135 (2013) 15986–15989.
[97] Y. Garcia, V. Niel, M. Carmen Muñoz, J.A. Real, Spin crossover in 1D, 2D and 3D polymeric fe(II) networks, Top. Curr. Chem. 233 (2004) 229–257.
[98] M.C. Muñoz, J.A. Real, Thermo-, piezo-, photo- and chemo-switchable spin crossover iron(II)-metallocyanate based coordination polymers, Coord. Chem. Rev. 255 (2011) 2068–2093.
[99] M.C. Muñoz, J.A. Real, M.A. Halcrow, Polymeric Spin-Crossover Materials, Spin-Crossover Mater. Prop. Appl., Wiley, 2013, pp. 121–138.
[100] J.G. Haasnoot, G. Vos, W.L. Groeneveld, 1, 2, 4-triazole complexes, III complexes of transition metal (II) nitrates and fluoroborates, Zeitschrift Für Naturforsch. B 32 (1977) 1421–1430.
[101] J.R. Galán-Mascarós, E. Coronado, A. Forment-Aliaga, M. Monrabal-Capilla, E. Pinilla-Cienfuegos, M. Ceolin, Tuning size and thermal hysteresis in bistable spin crossover nanoparticles, Inorg. Chem. 49 (2010) 5706–5714.
[102] M. Giménez-Marqués, M.L. García-Sanz de Larrea, E. Coronado, Unravelling the chemical design of spin-crossover nanoparticles based on iron(II)–triazole coordination polymers: towards a control of the spin transition, J. Mater. Chem. C 3 (2015) 7946–7953.
[103] T. Forestier, S. Mornet, N. Daro, T. Nishihara, S.I. Mouri, K. Tanaka, O. Fouché, E. Freysz, J.F. Létard, Nanoparticles of iron(II) spin-crossover, Chem. Commun. (2008) 4327–4329.
[104] F. Volatron, L. Catala, E. Rivie, A. Gloter, O. Ste, T. Mallah, Spin-crossover coordination nanoparticles, Inorg. Chem. 47 (2008) 6584–6586.
[105] I. Boldog, A.B. Gaspar, V. Martínez, P. Pardo-Ibañez, V. Ksenofontov, A. Bhattacharjee, P. Gütlich, J.A. Real, Spin-crossover nanocrystals with magnetic, optical, and structural bistability near room temperature, Angew. Chem. Int. Ed. 47 (2008) 6433–6437.
[106] J. Larionova, L. Salmon, Y. Guari, A. Tokarev, K. Molvinger, G. Molnár, A. Bousseksou, Towards the ultimate size limit of the memory effect in spin-crossover solids, Angew. Chem. Int. Ed. 120 (2008) 8360–8364.
[107] Y. Raza, F. Volatron, S. Moldovan, O. Ersen, V. Huc, C. Martini, F. Brisset, A. Gloter, O. Stéphan, A. Bousseksou, L. Catala, T. Mallah, Matrix-dependent cooperativity in spin crossover Fe(pyrazine)Pt(CN)4 nanoparticles, Chem. Commun. 47 (2011) 11501.
[108] S. Titos-Padilla, J.M. Herrera, X.W. Chen, J.J. Delgado, E. Colacio, Bifunctional hybrid SiO2 nanoparticles showing synergy between core spin crossover and shell luminescence properties, Angew. Chem. Int. Ed. 50 (2011) 3290–3293.
[109] J. Dugay, M. Giménez-Marqués, T. Kozlova, H.W. Zandbergen, E. Coronado, H. S.J. Van Der Zant, Spin switching in electronic devices based on 2D assemblies of spin-crossover nanoparticles, Adv. Mater. 27 (2015) 1288–1293.
[110] A. Holovchenko, J. Dugay, M. Giménez-Marqués, R. Torres-Cavanillas, E. Coronado, H.S.J. van der Zant, Near room-temperature memory devices based on hybrid spin-crossover@SiO_2 nanoparticles coupled to single-layer graphene nanoelectrodes, Adv. Mater. 28 (2016) 7228–7233.
[111] J. Dugay, M. Aarts, T. Kozlova, H.W. Zandbergen, E. Coronado, H.S.J. Van Der Zant, Phase transitions in spin-crossover thin films probed by graphene transport measurements, Nano Lett. 17 (2017) 186–193.
[112] J. Dugay, M. Giménez-Marqués, W.J. Venstra, R. Torres-Cavanillas, U.N. Sheombarsing, N. Manca, E. Coronado, H.S.J. Van Der Zant, Sensing of the molecular spin in spin-crossover nanoparticles with micromechanical resonators, J. Phys. Chem. C. 123 (2019) 6778–6786.
[113] R. Torres-Cavanillas, R. Sanchis-Gual, J. Dugay, M. Coronado-Puchau, M. Giménez-Marqués, E. Coronado, Design of bistable gold@spin-crossover core-shell nanoparticles showing large electrical responses for the spin switching, Adv. Mater. 31 (2019) 1900039.
[114] M. Piedrahita-Bello, J.E. Angulo-Cervera, A. Enriquez-Cabrera, G. Molnár, B. Tondu, L. Salmon, A. Bousseksou, Colossal expansion and fast motion in spin-crossover@polymer actuators, Mater. Horiz. 8 (2021) 3055–3062.
[115] R. Torres-Cavanillas, M. Morant-Giner, G. Escorcia-Ariza, J. Dugay, J. Canet-Ferrer, S. Tatay, S. Cardona-Serra, M. Giménez-Marqués, M. Galbiati, A. Forment-Aliaga, E. Coronado, Smart molecular/MoS2 heterostructures featuring light and thermally-induced strain driven by spin switching, Nat. Chem. 13 (2021) 1109–1120.
[116] L. Piñeiro-López, M. Seredyuk, M.C. Muñoz, J.A. Real, Effect of guest molecules on spin transition temperature in loaded Hofmann-like clathrates with improved porosity, Eur. J. Inorg. Chem. (2020) 764–769.
[117] Z.P. Ni, J.L. Liu, M.N. Hoque, W. Liu, J.Y. Li, Y.C. Chen, M.L. Tong, Recent advances in guest effects on spin-crossover behavior in Hofmann-type metal-organic frameworks, Coord. Chem. Rev. 335 (2017) 28–43.
[118] K. Otsubo, T. Haraguchi, H. Kitagawa, Nanoscale crystalline architectures of Hofmann-type metal–organic frameworks, Coord. Chem. Rev. 346 (2017) 123–138.
[119] C. Boix-Constant, V. García-López, E. Navarro-Moratalla, M. Clemente-León, J. L. Zafra, J. Casado, F. Guinea, S. Mañas-Valero, E. Coronado, Strain switching in van der waals heterostructures triggered by a spin-crossover metal-organic framework, Adv. Mater. 34 (2022) 2110027.
[120] Z.-H. Li, Y.-X. Wang, W.-K. Han, W. Zhu, T. Li, Z. Li, X. Ren, Z.-G. Gu, Integrating spin-crossover nanoparticles with silver nanowires: toward magnetic and conductive bifunctional nanomaterials, New J. Chem. 41 (2017) 10062–10068.
[121] M. Eddaoudi, J. Kim, N. Rosi, D. Vodak, J. Wachter, M. O'Keeffe, O.M. Yaghi, Systematic design of pore size and functionality in isoreticular MOFs and their application in methane storage, Science. 295 (2002) 469–472.
[122] K.M. Choi, D. Kim, B. Rungtaweevoranit, C.A. Trickett, J.T.D. Barmanbek, A.S. Alshammari, P. Yang, O.M. Yaghi, Plasmon-enhanced photocatalytic CO2 conversion within metal-organic frameworks under visible light, J. Am. Chem. Soc. 139 (2017) 356–362.
[123] B. Rungtaweevoranit, J. Baek, J.R. Araujo, B.S. Archanjo, K.M. Choi, O.M. Yaghi, G.A. Somorjai, Copper nanocrystals encapsulated in Zr-based metal-organic frameworks for highly selective CO2 hydrogenation to methanol, Nano Lett. 16 (2016) 7645–7649.
[124] M. Zhang, Y. Chen, J.-N. Chang, C. Jiang, W.-X. Ji, L.-Y. Li, M. Lu, L.-Z. Dong, S.-L. Li, Y.-P. Cai, Efficient charge migration in chemically-bonded Prussian blue analogue/CdS with beaded structure for photocatalytic H_2 evolution, JACS Au. 1 (2021) 212–220.
[125] E. Coronado, Molecular magnetism: from chemical design to spin control in molecules, materials and devices, Nat. Rev. Mater. 5 (2020) 87–104.
[126] G. Maurin-Pasturel, J. Long, Y. Guari, F. Godiard, M.G. Willinger, C. Guerin, J. Larionova, Nanosized heterostructures of Au@Prussian blue analogues:

Towards multifunctionality at the nanoscale, Angew. Chem. Int. Ed. 53 (2014) 3872–3876.
[127] R. Torres-Cavanillas, L. Lima-Moya, F.D. Tichelaar, H.W. Zandbergen, M. Giménez-Marqués, E. Coronado, Downsizing of robust Fe-triazole@SiO2 spin-crossover nanoparticles with ultrathin shells, Dalton Trans. 48 (2019) 15465–15469.
[128] E. Groeneveld, C. de Mello Donegá, The Challenge of Colloidal Nanoparticle Synthesis, in: Nanoparticles, Springer, 2014, pp. 145–189.
[129] S. Kalele, S.W. Gosavi, J. Urban, S.K. Kulkarni, Nanoshell particles: Synthesis, properties and applications, Curr. Sci. 91 (2006) 1038–1052.
[130] R. Sanchis-Gual, R. Torres-Cavanillas, M. Coronado-Puchau, M. Giménez-Marqués, E. Coronado, Plasmon-assisted spin transition in gold nanostar@spin crossover heterostructures, J. Mater. Chem. C. 9 (2021) 10811–10818.
[131] G. Zheng, S. de Marchi, V. López-Puente, K. Sentosun, L. Polavarapu, I. Pérez-Juste, E.H. Hill, S. Bals, L.M. Liz-Marzán, I. Pastoriza-Santos, J. Pérez-Juste, Encapsulation of single plasmonic nanoparticles within ZIF-8 and SERS analysis of the MOF flexibility, Small 12 (2016) 3935–3943.
[132] E. Prodan, C. Radloff, N.J. Halas, P. Nordlander, A hybridization model for the plasmon response of complex nanostructures, Science 302 (2003) 419–422.
[133] R. Purbia, S. Paria, Yolk/shell nanoparticles: Classifications, synthesis, properties, and applications, Nanoscale 7 (2015) 19789–19873.
[134] Z. Li, M. Li, Z. Bian, Y. Kathiraser, S. Kawi, Design of highly stable and selective core/yolk-shell nanocatalysts-review, Appl. Catal. B Environ. 188 (2016) 324–341.
[135] R. Cai, H. Jin, D. Yang, K. Te Lin, K. Chan, J. Sun, Z. Chen, X. Zhang, W. Tan, Generalized preparation of Au NP@Ni(OH)2 yolk-shell NPs and their enhanced catalytic activity, Nano Energy 71 (2020).
[136] C. Kuo, Y. Tang, L. Chou, B.T. Sneed, C.N. Brodsky, Z. Zhao, Yolk–shell nanocrystal@ZIF-8 nanostructures for gas-phase heterogeneous catalysis with selectivity control, J. Am. Chem. Soc. 134 (2012) 14345–14348.
[137] C. Wang, C. Xu, H. Zeng, S. Sun, Recent progress in syntheses and applications of dumbbell-like nanoparticles, Adv. Mater. 21 (2009) 3045–3052.
[138] J. Reguera, D. Jiménez De Aberasturi, M. Henriksen-Lacey, J. Langer, A. Espinosa, B. Szczupak, C. Wilhelm, L.M. Liz-Marzán, Janus plasmonic-magnetic gold-iron oxide nanoparticles as contrast agents for multimodal imaging, Nanoscale 9 (2017) 9467–9480.
[139] C. Wang, H. Yin, S. Dai, S. Sun, A general approach to noble metal-metal oxide dumbbell nanoparticles and their catalytic application for CO oxidation, Chem. Mater. 22 (2010) 3277–3282.
[140] R. Sanchis-Gual, I. Susic, R. Torres-Cavanillas, D. Arenas-Esteban, S. Bals, T. Mallah, M. Coronado-Puchau, E. Coronado, The design of magneto-plasmonic nanostructures formed by magnetic Prussian Blue-type nanocrystals decorated with Au nanoparticles, Chem. Commun. 57 (2021) 1903–1906.
[141] L. Moulet, N. Daro, S. Mornet, N. Vilar-Vidal, G. Chastanet, P. Guionneau, Grafting of gold onto spin-crossover nanoparticles: SCO@Au, Chem. Commun. 52 (2016) 13213–13216.
[142] G. Shemer, G. Markovich, Enhancement of magneto-optical effects in magnetite nanocrystals near gold surfaces, J. Phys. Chem. B. 106 (2002) 9195–9197.
[143] D. Qiu, L. Gu, X.-L. Sun, D.-H. Ren, Z.-G. Gu, Z. Li, SCO@SiO 2 @Au core–shell nanomaterials: enhanced photo-thermal plasmonic effect and spin-crossover properties, RSC Adv. 4 (2014) 61313–61319.
[144] I. Suleimanov, J. Sánchez Costa, G. Molnár, L. Salmon, A. Bousseksou, The photo-thermal plasmonic effect in spin crossover@silica–gold nanocomposites, Chem. Commun. 50 (2014) 13015–13018.
[145] F.N. Crespilho, V. Zucolotto, C.M.A. Brett, O.N. Oliveira, F.C. Nart, Enhanced charge transport and incorporation of redox mediators in layer-by-layer films containing PAMAM-encapsulated gold nanoparticles, J. Phys. Chem. B. 110 (2006) 17478–17483.
[146] M.H. Xue, Q. Xu, M. Zhou, J.J. Zhu, In situ immobilization of glucose oxidase in chitosan-gold nanoparticle hybrid film on Prussian Blue modified electrode for high-sensitivity glucose detection, Electrochem. Commun. 8 (2006) 1468–1474.
[147] N.B. Li, J.H. Park, K. Park, S.J. Kwon, H. Shin, J. Kwak, Characterization and electrocatalytic properties of Prussian blue electrochemically deposited on nano-Au/PAMAM dendrimer-modified gold electrode, Biosens. Bioelectron. 23 (2008) 1519–1526.
[148] S.S. Kumar, J. Joseph, K.L. Phani, Novel method for deposition of gold-prussian blue nanocomposite films induced by electrochemically formed gold nanoparticles: Characterization and application to electrocatalysis, Chem. Mater. 19 (2007) 4722–4730.
[149] J.D. Qiu, H.Z. Peng, R.P. Liang, J. Li, X.H. Xia, Synthesis, characterization, and immobilization of Prussian blue-modified au nanoparticles: Application to electrocatalytic reduction of H2O2, Langmuir 23 (2007) 2133–2137.
[150] C. Hong, R. Yuan, Y. Chai, Y. Zhuo, Amperometric immunosensor for the determination of ??-1-fetoprotein based on core-shell-shell Prussian blue-BSA-nanogold functionalized interface, Electroanalysis 20 (2008) 2185–2191.
[151] Y. Dou, X. Li, W. Yang, Y. Guo, M. Wu, Y. Liu, X. Li, X. Zhang, J. Chang, PB@Au core−satellite multifunctional nanotheranostics for magnetic resonance and computed tomography imaging in vivo and synergetic photothermal and radiosensitive therapy, ACS Appl. Mater. Interfaces 9 (2017) 1236–1272.
[152] L. Jing, X. Liang, Z. Deng, S. Feng, X. Li, M. Huang, Biomaterials Prussian blue coated gold nanoparticles for simultaneous photoacoustic/CT bimodal imaging and photothermal ablation of cancer, Biomaterials 35 (2014) 5814–5821.
[153] Y. Yin, Q. Li, S. Ma, H. Liu, B. Dong, J. Yang, D. Liu, Prussian Blue as a highly sensitive and background-free resonant Raman reporter, Anal. Chem. 89 (2017) 1551–1557.
[154] M. Li, J.Y. Wang, Q.Q. Chen, L.H. Lin, P. Radjenovic, H. Zhang, S.Y. Luo, Z.Q. Tian, J.F. Li, Background-free quantitative surface enhanced raman spectroscopy analysis using core-shell nanoparticles with an inherent internal standard, Anal. Chem. 91 (2019) 15025–15031.
[155] C. Zhang, Z. Xu, H. Di, E. Zeng, Y. Jiang, D. Liu, Gadolinium-doped Au@prussian blue nanoparticles as MR/SERS bimodal agents for dendritic cell activating and tracking, Theranostics 10 (2020) 6061–6071.
[156] N.R. Jana, L. Gearheart, S.O. Obare, C.J. Murphy, Anisotropic chemical reactivity of gold spheroids and nanorods, Langmuir 18 (2002) 922–927.
[157] G. Maurin-Pasturel, E. Rascol, M. Busson, S. Sevestre, J. Lai-Kee-Him, P. Bron, J. Long, J. Chopineau, J.-M. Devoisselle, Y. Guari, J. Larionova, ^{201} Tl-labeled Prussian blue and Au@Prussian blue nanoprobes for SPEC-CT imaging: influence of the size, shape and coating on the biodistribution, Inorg. Chem. Front. 4 (2017) 1737–1741.
[158] J. Larionova, G. Maurin-Pasturel, J. Long, M.A. Palacios, C. Guérin, C. Charnay, M.-G. Willinger, A.A. Trifonov, Y. Guari, Engineered Au core@Prussian Blue Analogues shell nanoheterostructures: their magnetic and optical properties, Chem. Eur. J. 23 (2017) 7483–7496.
[159] G. Maurin-Pasturel, E. Mamontova, M.A. Palacios, J. Long, J. Allouche, J.C. Dupin, Y. Guari, J. Larionova, Gold@Prussian blue analogue core-shell nanoheterostructures: Their optical and magnetic properties, Dalton Trans. 48 (2019) 6205–6216.
[160] D. Li, A. Bao, X. Chen, S. Li, T. Wang, L. Zhang, J. Ji, Q. Li, C. Wang, Y. Gao, Y. Yang, X. Dong, Prussian Blue@polyacrylic acid/Au aggregate janus nanoparticles for CT imaging-guided chemotherapy and enhanced photothermal therapy, Adv. Ther. 3 (2020) 2000091.
[161] E. Mamontova, M. Rodríguez-Castillo, E. Oliviero, Y. Guari, J. Larionova, M. Monge, J. Long, Designing heterostructured core@satellite Prussian Blue analogue@Au-Ag nanoparticles: Effect on the magnetic properties and catalytic activity, Inorg. Chem. Front. 8 (2021) 2248–2260.
[162] Y. Shi, Y. Shi, Z. Wang, J. Zhang, R. Hao, G. Zhang, X. Zhao, L. Zeng, Glucose-responsive mesoporous prussian blue nanoprobes coated with ultrasmall gold and manganese dioxide for magnetic resonance imaging and enhanced antitumor therapy, Chem. Eng. J. 453 (2023).
[163] L. Hang, H. Li, T. Zhang, D. Men, C. Zhang, P. Gao, Q. Zhang, Au@Prussian Blue hybrid nanomaterial synergy with a chemotherapeutic drug for tumor diagnosis and chemodynamic therapy, ACS Appl. Mater. Interfaces. 11 (2019) 39493–39502.
[164] R. Sanchis-Gual, T.F. Otero, M. Coronado-Puchau, E. Coronado, Enhancing the electrocatalytic activity and stability of Prussian blue analogues by increasing their electroactive sites through the introduction of Au nanoparticles, Nanoscale 13 (2021) 12676–12686.
[165] M. Zhang, W. Zhang, C. Engelbrekt, C. Hou, N. Zhu, Q. Chi, Size-dependent and self-catalytic gold@Prussian Blue nanoparticles for the electrochemical detection of hydrogen peroxide, ChemElectroChem 7 (2020) 3818–3823.
[166] C. Gu, L. Yang, M. Wang, N. Zhou, L. He, Z. Zhang, M. Du, A bimetallic (Cu-Co) Prussian Blue analogue loaded with gold nanoparticles for impedimetric aptasensing of ochratoxin a, Microchim. Acta 186 (2019) 343.
[167] S. Hermes, M.K. Schröter, R. Schmid, L. Khodeir, M. Muhler, A. Tissler, R.W. Fischer, R.A. Fischer, Metal@MOF: Loading of highly porous coordination polymers host lattices by metal organic chemical vapor deposition, Angew. Chem. Int. Ed. 44 (2005) 6237–6241.
[168] H.L. Jiang, B. Liu, T. Akita, M. Haruta, H. Sakurai, Q. Xu, Au@ZIF-8: CO oxidation over gold nanoparticles deposited to metal-organic framework, J. Am. Chem. Soc. 131 (2009) 11302–11303.
[169] X. Gu, Z.H. Lu, H.L. Jiang, T. Akita, Q. Xu, Synergistic catalysis of metal-organic framework-immobilized au-pd nanoparticles in dehydrogenation of formic acid for chemical hydrogen storage, J. Am. Chem. Soc. 133 (2011) 11822–11825.
[170] J. Juan-Alcañiz, J. Gascon, F. Kapteijn, Metal–organic frameworks as scaffolds for the encapsulation of active species: state of the art and future perspectives, J. Mater. Chem. 22 (2012) 10102–10118.
[171] M. Meilikhov, K. Yusenko, D. Esken, S. Turner, G. Van Tendeloo, R.A. Fischer, Metals@MOFs - Loading MOFs with metal nanoparticles for hybrid functions, Eur. J. Inorg. Chem. (2010) 3701–3714.
[172] P. Hu, J.V. Morabito, C.K. Tsung, Core-shell catalysts of metal nanoparticle core and metal-organic framework shell, ACS Catal. 4 (2014) 4409–4419.
[173] L. He, Y. Liu, J. Liu, Y. Xiong, J. Zheng, Y. Liu, Core – shell noble-metal@metal-organic-framework nanoparticles with highly selective sensing property, Angew. Chem. Int. Ed. 52 (2013) 3741–3745.
[174] K. Khaletskaya, J. Reboul, M. Meilikhov, M. Nakahama, S. Diring, M. Tsujimoto, S. Isoda, F. Kim, K.I. Kamei, R.A. Fischer, S. Kitagawa, S. Furukawa, Integration of porous coordination polymers and gold nanorods into core-shell mesoscopic composites toward light-induced molecular release, J. Am. Chem. Soc. 135 (2013) 10998–11005.
[175] P. Hu, J. Zhuang, L.Y. Chou, H.K. Lee, X.Y. Ling, Y.C. Chuang, C.K. Tsung, Surfactant-directed atomic to mesoscale alignment: Metal nanocrystals encased individually in single-crystalline porous nanostructures, J. Am. Chem. Soc. 136 (2014) 10561–10564.
[176] Z. Zhou, M. Li, J. Zhao, Z. Di, C. Di, B. Liu, C. Zhang, C.H. Yan, L. Li, Trace water mediated growth of oriented single-crystalline mesoporous metal-organic frameworks on gold nanorods, Chem. Commun. 54 (2018) 8182–8185.

[177] S. Dai, K.P. Ngoc, L. Grimaud, S. Zhang, A. Tissot, C. Serre, Impact of capping agent removal from Au NPs@MOF core-shell nanoparticle heterogeneous catalysts, J. Mater. Chem. A 10 (2022) 3201–3205.
[178] J.G. Hinman, J.G. Turner, D.M. Hofmann, C.J. Murphy, Layer-by-layer synthesis of conformal metal-organic framework shells on gold nanorods, Chem. Mater. 30 (2018) 7255–7261.
[179] X. Deng, S. Liang, X. Cai, S. Huang, Z. Cheng, Y. Shi, M. Pang, P. Ma, J. Lin, Yolk-shell structured Au nanostar@metal-organic framework for synergistic chemo-photothermal therapy in the second near-infrared window, Nano Lett. 19 (2019) 6772–6780.
[180] Y. Liu, W. Zhang, S. Li, C. Cui, J. Wu, H. Chen, F. Huo, Designable yolk–shell nanoparticle@MOF petalous heterostructures, Chem. Mater. 26 (2014) 1119–1125.
[181] N. Qin, A. Pan, J. Yuan, F. Ke, X. Wu, J. Zhu, J. Liu, J. Zhu, One-step construction of a hollow Au@bimetal-organic framework core-shell catalytic nanoreactor for selective alcohol oxidation reaction, ACS Appl. Mater. Interfaces. 13 (2021) 12463–12471.
[182] S. Yadnum, J. Roche, E. Lebraud, P. Négrier, P. Garrigue, D. Bradshaw, C. Warakulwit, J. Limtrakul, A. Kuhn, Site-selective synthesis of Janus-type metal-organic framework composites, Angew. Chem. Int. Ed. 126 (2014) 4082–4086.
[183] A. Ayala, C. Carbonell, I. Imaz, D. Maspoch, Introducing asymmetric functionality into MOFs: Via the generation of metallic Janus MOF particles, Chem. Commun. 52 (2016) 5096–5099.
[184] J. He, R.C.C. Yap, S. Yee Wong, Y. Zhang, Y. Hu, C. Chen, X. Zhang, J. Wang, X. Li, Controlled growth of a metal-organic framework on gold nanoparticles, CrystEngComm 18 (2016) 5262–5266.
[185] C.S. Hinde, W.R. Webb, B.K.J. Chew, R. Tan, W. Zhang, T.S.A. Hor, R. Raja, Utilisation of gold nanoparticles on amine-functionalised UiO-66 (NH2-UiO-66) nanocrystals for selective tandem catalytic reactions, Chem. Commun. 52 (2016) 6557–6560.
[186] T. Pan, I.E. Khalil, Z. Xu, H. Li, X. Zhang, G. Xiao, W. Zhang, Y. Shen, F. Huo, Spatial compartmentalization of metal nanoparticles within metal-organic frameworks for tandem reaction, Nano Res. 15 (2022) 1178–1182.
[187] Z. Gu, L. Chen, B. Duan, Q. Luo, J. Liu, C. Duan, Synthesis of Au@UiO-66(NH2) structures by small molecule-assisted nucleation for plasmon-enhanced photocatalytic activity, Chem. Commun. 52 (2016) 116–119.
[188] M. Wang, Y. Tang, Y. Jin, Modulating catalytic performance of metal-organic framework composites by localized surface plasmon resonance, ACS Catal. 9 (2019) 11502–11514.
[189] L.W. Chen, Y.C. Hao, Y. Guo, Q. Zhang, J. Li, W.Y. Gao, L. Ren, X. Su, L. Hu, N. Zhang, S. Li, X. Feng, L. Gu, Y.W. Zhang, A.X. Yin, B. Wang, Metal-organic framework membranes encapsulating gold nanoparticles for direct plasmonic photocatalytic nitrogen fixation, J. Am. Chem. Soc. 143 (2021) 5727–5736.
[190] M. Izadpanah Ostad, M. Niknam Shahrak, F. Galli, The effect of different reaction media on photocatalytic activity of Au- and Cu-decorated zeolitic imidazolate Framework-8 toward CO2 photoreduction to methanol, J. Solid State Chem. 315 (2022).
[191] D.K. Yadav, V. Ganesan, P.K. Sonkar, R. Gupta, P.K. Rastogi, Electrochemical investigation of gold nanoparticles incorporated zinc based metal-organic framework for selective recognition of nitrite and nitrobenzene, Electrochim. Acta 200 (2016) 276–282.
[192] H. Chen, T. Yang, F. Liu, W. Li, Electrodeposition of gold nanoparticles on Cu-based metal-organic framework for the electrochemical detection of nitrite, Sens. Actuators, B Chem. 286 (2019) 401–407.
[193] Y. Wang, L. Wang, H. Chen, X. Hu, S. Ma, Fabrication of highly sensitive and stable hydroxylamine electrochemical sensor based on gold nanoparticles and metal-metalloporphyrin framework modified electrode, ACS Appl. Mater. Interfaces 8 (2016) 18173–18181.
[194] K.V. Kavya, S. Vargheese, D. Pattappan, R.T. Rajendra Kumar, Y. Haldorai, Screen-printed electrode modified by Au/NH2-MIL-125(Ti) composite for electrochemical sensing performance of gallic acid in green tea and urine samples, Chem. Phys. Lett. 807 (2022).
[195] X. Liu, L. Chen, Y. Gao, J. Li, J. Sun, T. Gan, Molecularly imprinted polymer capped Au@HKUST-1 nanocapsules-based electrochemical sensing platform for monitoring isoproturon herbicide in water at sub-nanomole level, J. Environ. Chem. Eng. 10 (2022).
[196] W. Lin, C.J. Murphy, A demonstration of le Chatelier's principle on the nanoscale, ACS Cent. Sci. 3 (2017) 1096–1102.
[197] Y. Li, J. Jin, D. Wang, J. Lv, K. Hou, Y. Liu, C. Chen, Coordination-responsive drug release inside gold nanorod @ metal-organic framework core–shell nanostructures for near-infrared-induced synergistic chemo-photothermal therapy, Nano Res. 11 (2018) 3294–3305.
[198] J.Y. Zeng, M.K. Zhang, M.Y. Peng, D. Gong, X.Z. Zhang, Porphyrinic metal-organic frameworks coated gold nanorods as a versatile nanoplatform for combined photodynamic/photothermal/chemotherapy of tumor, Adv. Funct. Mater. 28 (2018) 1705451.
[199] C. Carrillo-Carrión, R. Martínez, M.F. Navarro Poupard, B. Pelaz, E. Polo, A. Arenas-Vivo, A. Olgiati, P. Taboada, M.G. Soliman, Ú. Catalán, S. Fernández-Castillejo, R. Solà, W.J. Parak, P. Horcajada, R.A. Alvarez-Puebla, P. del Pino, Aqueous stable gold nanostar/ZIF-8 nanocomposites for light-triggered release of active cargo inside living cells, Angew. Chem. Int. Ed. 58 (2019) 7078–7082.
[200] W. Shang, C. Zeng, Y. Du, H. Hui, X. Liang, C. Chi, K. Wang, Z. Wang, J. Tian, Core-shell gold nanorod@metal–organic framework nanoprobes for multimodality diagnosis of glioma, Adv. Mater. 29 (2017) 1604381.
[201] Y. Hu, J. Liao, D. Wang, G. Li, Fabrication of gold nanoparticle-embedded metal-organic framework for highly sensitive surface-enhanced Raman scattering detection, Anal. Chem. 86 (2014) 3955–3963.
[202] Z. Zhou, J. Zhao, Z. Di, B. Liu, Z. Li, X. Wu, L. Li, Core-shell gold nanorod@mesoporous-MOF heterostructures for combinational phototherapy, Nanoscale 13 (2021) 131–137.
[203] C.S.L. Koh, H.K. Lee, X. Han, H.Y.F. Sim, X.Y. Ling, Plasmonic nose: integrating the MOF-enabled molecular preconcentration effect with a plasmonic array for recognition of molecular-level volatile organic compounds, Chem. Commun. 54 (2018) 2546–2549.
[204] X. Cao, S. Hong, Z. Jiang, Y. She, S. Wang, C. Zhang, H. Li, F. Jin, M. Jin, J. Wang, SERS-active metal–organic frameworks with embedded gold nanoparticles, Analyst 142 (2017) 2640–2647.
[205] Y.A. Tobon, C. Etrillard, O. Nguyen, J.F. Létard, V. Faramarzi, J.F. Dayen, B. Doudin, D.M. Bassani, F. Guillaume, Resonance Raman study of spin-crossover [Fe(Htrz)2(trz)](BF 4)·H2O particles coated with gold, Eur. J. Inorg. Chem. 2 (2012) 5837–5842.
[206] K. Abdul-Kader, M. Lopes, C. Bartual-Murgui, O. Kraieva, E.M. Hernández, L. Salmon, W. Nicolazzi, F. Carcenac, C. Thibault, G. Molnár, A. Bousseksou, Synergistic switching of plasmonic resonances and molecular spin states, Nanoscale 5 (2013) 5288.
[207] Y. Hu, M. Picher, N.M. Tran, M. Palluel, L. Stoleriu, N. Daro, S. Mornet, C. Enachescu, E. Freysz, F. Banhart, G. Chastanet, Photo-thermal switching of individual plasmonically activated spin crossover nanoparticle imaged by ultrafast transmission electron microscopy, Adv. Mater. 33 (2021) 2105586.